

An Adaptive Hierarchical Control for Aerial Manipulators

Francesco Pierri *, Giuseppe Muscio and Fabrizio Caccavale

Università degli Studi della Basilicata, Scuola di Ingegneria, via dell'Ateneo Lucano 10, 85100, Potenza, Italy

(Accepted MONTH DAY, YEAR. First published online: MONTH DAY, YEAR)

SUMMARY

This paper addresses the trajectory tracking control problem for a quadrotor aerial vehicle, equipped with a robotic manipulator (aerial manipulator). The controller is organized in two layers: in the top layer, an inverse kinematics algorithm computes the motion references for the actuated variables; in the bottom layer, a motion control algorithm is in charge of tracking the motion references computed by the upper layer. To the purpose, a model-based control scheme is adopted, where modeling uncertainties are compensated through an adaptive term. The stability of the proposed scheme is proven by resorting to Lyapunov arguments. Finally, a simulation case study is proposed to prove the effectiveness of the approach.

KEYWORDS: Aerial Manipulation; Adaptive Control; Model-Based Control.

1. Introduction

Over the last years, Unmanned Aerial Vehicles (UAVs) have witnessed a scientific community interest, due to the developments in sensors and communication that make UAVs more suitable for a large number of applications, such as surveillance and remote monitoring,¹ cooperative transportation,² rescue missions³ and monitoring of hostile environments.⁴

Among UAVs, there is a great interest for Vertical Takeoff and Landing (VTOL) vehicles, such as multirotor helicopters. Motion control of multirotors is a widely investigated but still challenging issue, since they are under-actuated systems and, often, are equipped with limited sensing devices. Conventional approaches to UAV control have been based on linear controller design⁵ and robust \mathcal{H}_∞ controllers, requiring model linearization about a set of equilibrium conditions.⁶ Linear controllers are characterized by satisfactory performance near the design conditions or in hovering, but performance degradation is usually observed when the aircraft moves away from these conditions. To overcome these drawbacks, many nonlinear controllers have been proposed, including model predictive control,⁷ backstepping⁸ and sliding mode techniques.⁹ Recently, adaptive control laws have been proposed, e.g., in [10], where a feedback linearization approach is adopted and the mathematical model of the UAV is written in such a way to point out its linear dependency on the position of the center of gravity. In [11], the effect of constant exogenous forces and moments, and the presence of unknown dynamic parameters (e.g., the position of the center of mass) have been considered. Since it is possible to make a conceptual separation between position and orientation of a quadrotor, hierarchical controllers, based on an inner-outer loop, have been successfully proposed as, e.g., in [12].

A relatively recent application field is aerial manipulation by means of UAVs equipped with grippers or robotic arms. This is a challenging issue since the vehicle is characterized

* Corresponding author. E-mail: francesco.pierri@unibas.it

by unstable dynamics and the presence of the gripper/arm, as well as the held object, can cause nontrivial coupling effects.¹³ Different mechanical structures have been added to the aerial vehicle: in [13] a compliant gripper, composed of four fingers, is proposed, while in [14] several light-weight low-complexity grippers are tested. More recently, in order to extend their manipulation capabilities, research platforms including multi-DOFs manipulators mounted on VTOL UAVs have been developed (aerial manipulators, see [15] for a brief literature review). The manipulator's motion generates reaction forces on the UAV that can have destabilizing effects.¹⁶ The problem of interaction between the arm and the vehicle has been tackled in [17] and [18], where the dynamic coupling of an helicopter with a 7-DOFs robotic manipulator is analyzed, while in [19] an adaptive scheme, aimed at compensating the manipulator's mass and the interaction caused by its movements, is proposed. In [20], the authors present the design, modeling and control of an aerial manipulator consisting of a quadrotor helicopter endowed with a robotic manipulator based on a 3-DOFs delta structure and a 3-DOFs end-effector. In [21], an adaptive controller for a quadrotor equipped with a 2-DOFs manipulator is designed and experimentally validated. In [22], a model reference adaptive control is proposed for a light-weight prototype 3-arm manipulator, each arm with 2 DOFs. In [23] and [24], a Cartesian impedance control is developed to counteract the effects of contact forces and external disturbances.

Hierarchical control of aerial manipulators to perform tasks in operational space has been introduced in [25], where a model-based control approach is pursued, and in [26], where model-free motion control laws are adopted. The algorithm in [25] has been extended via an adaptive term for compensating the model uncertainties.²⁷

In this paper, the problem of motion control of the end-effector of a robot manipulator mounted on a quadrotor helicopter is tackled through a hierarchical control architecture. Differently from UAVs not equipped by arms, the position and attitude dynamics are not decoupled,¹² due to the presence of the arm. Thus, in order to cope with this aspect, an adaptive solution is proposed. In the top layer, an inverse kinematics algorithm computes the motion references for the actuated variables, i.e., position and yaw angle of the vehicle and joint variables for the manipulator. In the bottom layer, an adaptive model-based motion control algorithm is in charge of tracking the motion references: a vehicle position controller computes the thrust force and the reference values for pitch and roll angles; then, an attitude controller, on the basis of the pitch-roll references, computes the moments acting on the quadrotor, while the manipulator controller computes the joint torques. It is worth remarking that the model adopted to design the proposed control law does not include some inertial coupling terms; this choice allows to decouple the design the quadrotor position and attitude controllers. Therefore, the adaptive term not only allows to cope with unavoidable modeling uncertainties, but also to counteract the effect of the dynamical terms intentionally neglected in the design of the control law. Moreover, a rigorous stability analysis of the system is carried out via Lyapunov arguments. Finally, in order to prove the effectiveness of the approach, a simulation case study has been developed, by considering a dynamic model of the aerial manipulator, that has been validated on a real setup.²⁸ In order to make the simulation more realistic, some non-idealities, like sensor noise, modeling uncertainties and aerodynamic disturbances, have been also considered. The performance of the proposed controlled is compared with that of a PID controller.²⁹

Preliminary results related to the proposed control scheme have been presented in [25] and [27]. More in detail, the two-loop scheme was firstly introduced in [25], in a preliminary version, without the adaptive term and a first order kinematic inversion algorithm. The scheme was improved in [27], where the adaptive term is added as well as a second-order inverse kinematic algorithm. Here, the adaptive scheme has been inherited from [27], and a rigorous theoretical analysis has been added: in detail, the exponential stability of both inner and outer loops, which, in turn, is crucial to prove the stability of the whole two-loop scheme, is proven, as well as the asymptotic convergence of the two loops scheme, that were simply claimed but not rigorously proven in [27].

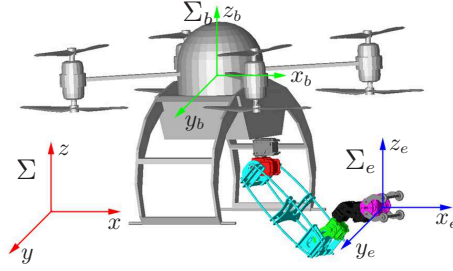


Fig. 1. Quadrotor and robotic arm system with the corresponding reference frames.

The paper is organized as follows: in Section 2 the kinematic and dynamic models of the aerial manipulator are presented, in Section 3 the control architecture is described, in Section 4 a method for estimating the uncertainties is provided, while in Section 5 the stability of the closed-loops dynamics is proven. Finally, Section 6 reports the simulation results, while Section 7 presents some conclusive considerations.

2. Modeling

A quadrotor helicopter is a Vertical Takeoff and Landing (VTOL) rotorcraft with 4 propellers, whose axes are aligned to the same direction. The propeller of each rotor generates a force and the total thrust is given by the sum of the individual forces. Therefore, the quadrotor is an under-actuated vehicle with four input forces and six degrees of freedom (DOFs), describing the position and orientation of the vehicle center of mass. Two of the rotors rotate in clockwise direction, while the other two are counterclockwise. The basic motions are generated by varying the thrust of the single rotors: pitch and roll movements are obtained by assigning different thrusts to two concordant rotors, while yaw movement is given by different thrust between the two couple of rotors. Vertical motion is obtained by changing the total thrust of all rotors.

The system considered in this paper, depicted in Fig. 1, is composed of a quadrotor vehicle equipped with a n -DOF robotic arm characterized by all revolute joints.

2.1. Kinematics

Let Σ_b denote the vehicle body-fixed reference frame with origin at the vehicle center of mass; its position with respect to the world fixed inertial reference frame, Σ , is given by the (3×1) vector \mathbf{p}_b , while its orientation is given by the rotation matrix \mathbf{R}_b

$$\mathbf{R}_b(\boldsymbol{\phi}_b) = \begin{bmatrix} c_\psi c_\theta & c_\psi s_\theta s_\varphi & -s_\psi c_\varphi & c_\psi s_\theta c_\varphi & + s_\psi s_\varphi \\ s_\psi c_\theta & s_\psi s_\theta s_\varphi & + c_\psi c_\varphi & s_\psi s_\theta c_\varphi & - c_\psi s_\varphi \\ -s_\theta & c_\theta s_\varphi & & c_\theta c_\varphi & \end{bmatrix}, \quad (1)$$

where $\boldsymbol{\phi}_b = [\psi \ \theta \ \varphi]^T$ is the triple of ZYX yaw-pitch-roll angles and c_* and s_* denote, respectively, $\cos(*)$ and $\sin(*)$ ($*$ = ψ, θ, φ).

Let Σ_e be the frame attached to the end effector of the manipulator (Fig. 1). The position of Σ_e with respect to Σ is given by

$$\mathbf{p}_e = \mathbf{p}_b + \mathbf{R}_b \mathbf{p}_{eb}^b, \quad (2)$$

where the vector \mathbf{p}_{eb}^b describes the position of Σ_e with respect to Σ_b expressed in frame Σ_b . The linear velocity $\dot{\mathbf{p}}_e$ of Σ_e in the fixed frame is obtained by differentiating (2), i.e.,

$$\dot{\mathbf{p}}_e = \dot{\mathbf{p}}_b - \mathbf{S}(\mathbf{R}_b \mathbf{p}_{eb}^b) \boldsymbol{\omega}_b + \mathbf{R}_b \dot{\mathbf{p}}_{eb}^b, \quad (3)$$

where $\mathbf{S}(\cdot)$ is the (3×3) skew-symmetric matrix operator performing the cross product.³⁰ The orientation of Σ_e can be described by the rotation matrix

$$\mathbf{R}_e = \mathbf{R}_b \mathbf{R}_e^b, \quad (4)$$

where \mathbf{R}_e^b describes the orientation of Σ_e with respect to Σ_b . The angular velocity $\boldsymbol{\omega}_e$ of Σ_e is given by

$$\boldsymbol{\omega}_e = \boldsymbol{\omega}_b + \mathbf{R}_b \boldsymbol{\omega}_{eb}^b, \quad (5)$$

where $\boldsymbol{\omega}_{eb}^b = \mathbf{R}_b^\top (\boldsymbol{\omega}_e - \boldsymbol{\omega}_b)$ is the relative angular velocity between Σ_e and Σ_b , expressed in the frame Σ_b .

Let \mathbf{q} be the $(n \times 1)$ vector of positions of the manipulator joints, then, $\mathbf{p}_{eb}^b(\mathbf{q})$ and $\mathbf{R}_e^b(\mathbf{q})$ can be viewed as the direct kinematics equations of a ground-fixed manipulator with respect to its base frame, Σ_b . The (6×1) vector of the generalized velocity of the end-effector with respect to Σ_b , $\mathbf{v}_{eb}^b = [\dot{\mathbf{p}}_{eb}^{b\top} \boldsymbol{\omega}_{eb}^{b\top}]^\top$, can be written in terms of the joint velocities $\dot{\mathbf{q}}$ via the manipulator geometric Jacobian, \mathbf{J}_{eb}^b , expressed in frame Σ_b , i.e.,

$$\mathbf{v}_{eb}^b = \mathbf{J}_{eb}^b(\mathbf{q}) \dot{\mathbf{q}}. \quad (6)$$

On the basis of (3), (5) and (6), the generalized end-effector velocity, $\mathbf{v}_e = [\dot{\mathbf{p}}_e^\top \boldsymbol{\omega}_e^\top]^\top$, can be expressed as

$$\mathbf{v}_e = \mathbf{J}_b(\mathbf{q}, \mathbf{R}_b) \mathbf{v}_b + \mathbf{J}_{eb}(\mathbf{q}, \mathbf{R}_b) \dot{\mathbf{q}}, \quad (7)$$

where $\mathbf{v}_b = [\dot{\mathbf{p}}_b^\top \boldsymbol{\omega}_b^\top]^\top$ is the generalized velocity of the vehicle frame,

$$\mathbf{J}_b = \begin{bmatrix} \mathbf{I}_3 & -\mathbf{S}(\mathbf{R}_b \mathbf{p}_{eb}^b) \\ \mathbf{O}_3 & \mathbf{I}_3 \end{bmatrix},$$

and \mathbf{J}_{eb} is the manipulator Jacobian expressed in the inertial frame, i.e.,

$$\mathbf{J}_{eb} = \begin{bmatrix} \mathbf{R}_b & \mathbf{O}_3 \\ \mathbf{O}_3 & \mathbf{R}_b \end{bmatrix} \mathbf{J}_{eb}^b,$$

with \mathbf{I}_m and \mathbf{O}_m denoting the $(m \times m)$ identity and null matrices, respectively.

Usually, the attitude of the vehicle is expressed in terms of yaw-pitch-roll angles; in this case equation (7), in terms of the operational space vector $\mathbf{x}_b = [\mathbf{p}_b^\top, \boldsymbol{\phi}_b^\top]^\top$, becomes

$$\mathbf{v}_e = \mathbf{J}_b(\mathbf{q}, \boldsymbol{\phi}_b) \mathbf{T}_A(\boldsymbol{\phi}_b) \dot{\mathbf{x}}_b + \mathbf{J}_{eb}(\mathbf{q}, \mathbf{R}_b) \dot{\mathbf{q}}, \quad (8)$$

with

$$\mathbf{T}_A(\boldsymbol{\phi}_b) = \begin{bmatrix} \mathbf{I}_3 & \mathbf{O}_3 \\ \mathbf{O}_3 & \mathbf{T}(\boldsymbol{\phi}_b) \end{bmatrix}, \quad \mathbf{T}(\boldsymbol{\phi}_b) = \begin{bmatrix} 0 & -s_\psi & c_\psi c_\theta \\ 0 & c_\psi & s_\psi c_\theta \\ 1 & 0 & -s_\theta \end{bmatrix}, \quad (9)$$

where $\mathbf{T}(\boldsymbol{\phi}_b)$ is the transformation matrix between the angular velocity $\boldsymbol{\omega}_b$ and the time derivative of the Euler angles $\dot{\boldsymbol{\phi}}_b$.³⁰

Since the quadrotor vehicle is an under-actuated system, i.e., only 4 independent control inputs are available against the 6 DOFs, the position and the yaw angle are usually the controlled variables, while pitch and roll angles are used as intermediate

control inputs for position control. Hence, it is worth rewriting the vector \mathbf{x}_b as follows

$$\mathbf{x}_b = \begin{bmatrix} \boldsymbol{\eta}_b \\ \boldsymbol{\sigma}_b \end{bmatrix}, \quad \boldsymbol{\eta}_b = \begin{bmatrix} \mathbf{p}_b \\ \psi \end{bmatrix}, \quad \boldsymbol{\sigma}_b = \begin{bmatrix} \theta \\ \varphi \end{bmatrix}.$$

Thus, the differential kinematics (8) becomes

$$\begin{aligned} \mathbf{v}_e &= \mathbf{J}_\eta(\mathbf{q}, \boldsymbol{\phi}_b) \dot{\boldsymbol{\eta}}_b + \mathbf{J}_\sigma(\mathbf{q}, \boldsymbol{\phi}_b) \dot{\boldsymbol{\sigma}}_b + \mathbf{J}_{eb}(\mathbf{q}, \boldsymbol{\phi}_b) \dot{\mathbf{q}} \\ &= \mathbf{J}_\zeta(\boldsymbol{\sigma}_b, \boldsymbol{\zeta}) \dot{\boldsymbol{\zeta}} + \mathbf{J}_\sigma(\boldsymbol{\sigma}_b, \boldsymbol{\zeta}) \dot{\boldsymbol{\sigma}}_b, \end{aligned} \quad (10)$$

where $\boldsymbol{\zeta} = [\boldsymbol{\eta}_b^\top \mathbf{q}^\top]^\top$ is the vector of controlled variables, \mathbf{J}_η is composed of the first 4 columns of $\mathbf{J}_b \mathbf{T}_A(\boldsymbol{\phi}_b)$, \mathbf{J}_σ is composed of the last 2 columns of $\mathbf{J}_b \mathbf{T}_A(\boldsymbol{\phi}_b)$ and $\mathbf{J}_\zeta = [\mathbf{J}_\eta \ \mathbf{J}_{eb}]$.

2.2. Dynamics

The dynamic model of the system can be written as

$$\mathbf{M}(\boldsymbol{\xi}) \ddot{\boldsymbol{\xi}} + \mathbf{C}(\boldsymbol{\xi}, \dot{\boldsymbol{\xi}}) \dot{\boldsymbol{\xi}} + \mathbf{g}(\boldsymbol{\xi}) + \mathbf{d}(\boldsymbol{\xi}, \dot{\boldsymbol{\xi}}) = \mathbf{u}, \quad (11)$$

where $\boldsymbol{\xi} = [\mathbf{p}_b^\top \boldsymbol{\phi}_b^\top \mathbf{q}^\top]^\top \in \mathbb{R}^{6+n}$, \mathbf{M} represents the symmetric and positive definite inertia matrix of the system, \mathbf{C} is the matrix of Coriolis and centrifugal terms, \mathbf{g} is the vector of gravity generalized forces, \mathbf{d} takes into account disturbances, such as aerodynamic effects, and modeling uncertainties. The vector of inputs, \mathbf{u} , is given by

$$\mathbf{u} = \begin{bmatrix} \mathbf{u}_f \\ \mathbf{u}_\mu \\ \mathbf{u}_\tau \end{bmatrix} = \begin{bmatrix} \mathbf{R}_b(\boldsymbol{\phi}_b) \mathbf{f}_b^b \\ \mathbf{T}^\top(\boldsymbol{\phi}_b) \mathbf{R}_b(\boldsymbol{\phi}_b) \boldsymbol{\mu}_b^b \\ \boldsymbol{\tau} \end{bmatrix}, \quad (12)$$

where $\boldsymbol{\tau}$ is the $(n \times 1)$ vector of the manipulator joint torques, while $\mathbf{f}_b^b = [0 \ 0 \ f_z]^\top$ and $\boldsymbol{\mu}_b^b = [\mu_\psi \ \mu_\theta \ \mu_\varphi]^\top$ are, respectively, the forces and the torques generated by the 4 motors of the quadrotor, expressed in the frame Σ_b . Both f_z and $\boldsymbol{\mu}_b^b$ are related to the four actuation forces, output by the quadrotor motors, \mathbf{f} , via³¹

$$\begin{bmatrix} f_z \\ \boldsymbol{\mu}_b^b \end{bmatrix} = \begin{bmatrix} 1 & 1 & 1 & 1 \\ 0 & l_2 & 0 & -l_4 \\ -l_1 & 0 & l_3 & 0 \\ c & -c & c & -c \end{bmatrix} \begin{bmatrix} f_1 \\ f_2 \\ f_3 \\ f_4 \end{bmatrix} = \boldsymbol{\Gamma} \mathbf{f}, \quad (13)$$

where $l_i > 0$, $(i = 1, 2, 3, 4)$ is the distance from the i th motor and the vehicle center of mass, $c = \gamma_d / \gamma_t$, and γ_d , γ_t are the drag and thrust coefficient, respectively.

The matrices introduced in (11) can be detailed by considering the expressions derived in [23]. The inertia matrix can be viewed as a block matrix

$$\mathbf{M}(\boldsymbol{\xi}) = \begin{bmatrix} \mathbf{M}_{pp} & \mathbf{M}_{p\phi} & \mathbf{M}_{pq} \\ \mathbf{M}_{p\phi}^\top & \mathbf{M}_{\phi\phi} & \mathbf{M}_{\phi q} \\ \mathbf{M}_{pq}^\top & \mathbf{M}_{\phi q}^\top & \mathbf{M}_{qq} \end{bmatrix}, \quad (14)$$

where $\mathbf{M}_{pp} \in \mathbb{R}^{3 \times 3}$, $\mathbf{M}_{p\phi} \in \mathbb{R}^{3 \times 3}$, $\mathbf{M}_{pq} \in \mathbb{R}^{3 \times n}$, $\mathbf{M}_{\phi\phi} \in \mathbb{R}^{3 \times 3}$, $\mathbf{M}_{\phi q} \in \mathbb{R}^{3 \times n}$ and $\mathbf{M}_{qq} \in \mathbb{R}^{n \times n}$.

Similarly, matrix \mathbf{C} , vectors \mathbf{g} and \mathbf{d} in (11) can be partitioned as

$$\mathbf{C}(\boldsymbol{\xi}, \dot{\boldsymbol{\xi}}) = \begin{bmatrix} \mathbf{C}_p \\ \mathbf{C}_\phi \\ \mathbf{C}_q \end{bmatrix}, \quad \mathbf{g}(\boldsymbol{\xi}) = \begin{bmatrix} \mathbf{g}_p \\ \mathbf{g}_\phi \\ \mathbf{g}_q \end{bmatrix}, \quad \mathbf{d}(\boldsymbol{\xi}, \dot{\boldsymbol{\xi}}) = \begin{bmatrix} \mathbf{d}_p \\ \mathbf{d}_\phi \\ \mathbf{d}_q \end{bmatrix},$$

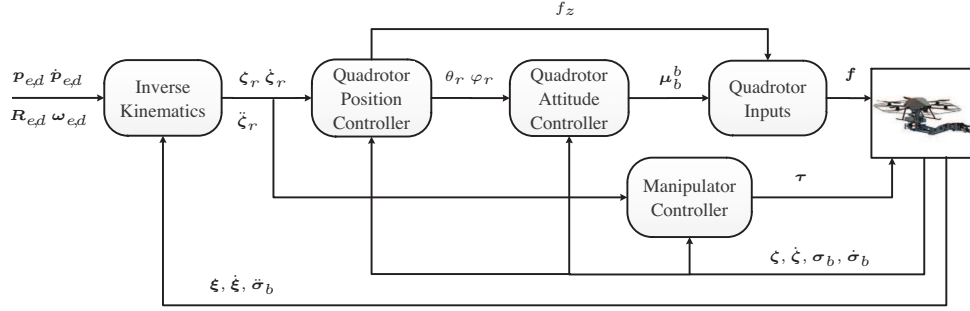


Fig. 2. Block scheme of the control architecture

with $C_p \in \mathbb{R}^{3 \times (6+n)}$, $C_\phi \in \mathbb{R}^{3 \times (6+n)}$, $C_q \in \mathbb{R}^{n \times (6+n)}$ and $\mathbf{g}_p, \mathbf{d}_p \in \mathbb{R}^3$, $\mathbf{g}_\phi, \mathbf{d}_\phi \in \mathbb{R}^3$ and $\mathbf{g}_q, \mathbf{d}_q \in \mathbb{R}^n$.

It is worth remarking that the inertia matrix, the Coriolis and gravity terms in (11) take into account the dynamic and static coupling between the platform and the arm.²³

3. Control Scheme

A task for the aerial manipulator is usually specified in terms of a desired trajectory for the end-effector position, $\mathbf{p}_{e,d}(t)$, and orientation, $\mathbf{R}_{e,d}(t)$; the corresponding desired linear and angular velocities (accelerations), $\dot{\mathbf{p}}_{e,d}(t)$ ($\ddot{\mathbf{p}}_{e,d}(t)$) and $\boldsymbol{\omega}_{e,d}(t)$ ($\dot{\boldsymbol{\omega}}_{e,d}(t)$), must be also assigned. The proposed hierarchical control strategy is composed of two layers. In the top layer, an inverse kinematics algorithm computes the motion references, in terms of reference values for position, velocities and acceleration of the quadrotor and the arm joints. Then, in the bottom layer, a motion control algorithm is designed in such a way that $\boldsymbol{\eta}_b$ and \mathbf{q} track the corresponding reference trajectories, $\boldsymbol{\eta}_r$ and \mathbf{q}_r , output by the top layer. The whole scheme is summarized in Fig. 2. In the following, it is assumed that $\dim\{\boldsymbol{\zeta}\} = n + 4 \geq \dim\{\mathbf{v}_e\} = 6$, i.e., the number of DOFs characterizing the aerial manipulator is, at least, equal to the dimension of the assigned task.

3.1. Inverse Kinematics

The time derivative of the differential kinematics (10), given by

$$\dot{\mathbf{v}}_e = \dot{\mathbf{J}}_\zeta(\boldsymbol{\sigma}_b, \boldsymbol{\zeta})\dot{\boldsymbol{\zeta}} + \mathbf{J}_\zeta(\boldsymbol{\sigma}_b, \boldsymbol{\zeta})\ddot{\boldsymbol{\zeta}} + \dot{\mathbf{J}}_\sigma(\boldsymbol{\sigma}_b, \boldsymbol{\zeta})\dot{\boldsymbol{\sigma}}_b + \mathbf{J}_\sigma(\boldsymbol{\sigma}_b, \boldsymbol{\zeta})\ddot{\boldsymbol{\sigma}}_b, \quad (15)$$

is considered to derive a second order closed-loop inverse kinematics algorithm,³² in charge of computing the trajectory references for the motion control loops at the bottom layer

$$\ddot{\boldsymbol{\zeta}}_r = \mathbf{J}_\zeta^\dagger(\boldsymbol{\sigma}_b, \boldsymbol{\zeta}) (\dot{\mathbf{v}}_{e,d} + \mathbf{K}_v(\mathbf{v}_{e,d} - \mathbf{v}_e) + \mathbf{K}_p \mathbf{e}) - \mathbf{J}_\zeta^\dagger(\boldsymbol{\sigma}_b, \boldsymbol{\zeta}) (\dot{\mathbf{J}}_\zeta(\boldsymbol{\sigma}_b, \boldsymbol{\zeta})\dot{\boldsymbol{\zeta}} + \mathbf{J}_\sigma(\boldsymbol{\sigma}_b, \boldsymbol{\zeta})\dot{\boldsymbol{\sigma}}_b + \dot{\mathbf{J}}_\sigma(\boldsymbol{\sigma}_b, \boldsymbol{\zeta})\dot{\boldsymbol{\sigma}}_b), \quad (16)$$

where $\mathbf{J}_\zeta^\dagger = \mathbf{J}_\zeta^T (\mathbf{J}_\zeta \mathbf{J}_\zeta^T)^{-1}$ is a right pseudoinverse of \mathbf{J}_ζ , \mathbf{e} is the error between the desired and the actual end-effector pose, \mathbf{K}_v and \mathbf{K}_p are symmetric positive definite gain matrices, given by

$$\mathbf{K}_p = \begin{bmatrix} \mathbf{K}_{p,P} \\ \mathbf{K}_{p,O} \end{bmatrix}, \quad \mathbf{K}_v = \begin{bmatrix} \mathbf{K}_{v,P} \\ \mathbf{K}_{v,O} \end{bmatrix} = \begin{bmatrix} \mathbf{K}_{v,P} \\ k_{v,O} \mathbf{I}_3 \end{bmatrix}, \quad (17)$$

with $k_{v,O}$ a positive constant.

Since the unit quaternion is used to represent the end-effector orientation, the pose error can be computed as³³

$$\mathbf{e} = \begin{bmatrix} \mathbf{e}_P \\ \mathbf{e}_O \end{bmatrix} = \begin{bmatrix} \mathbf{p}_{e,d} - \mathbf{p}_e(\boldsymbol{\sigma}_b, \boldsymbol{\zeta}) \\ \tilde{\boldsymbol{\epsilon}}(\boldsymbol{\sigma}_b, \boldsymbol{\zeta}) \end{bmatrix}, \quad (18)$$

where $\tilde{\boldsymbol{\epsilon}}$ is the vector part of the unit quaternion, $\tilde{\mathcal{Q}} = \{\tilde{\eta}, \tilde{\boldsymbol{\epsilon}}\}$ (with $\tilde{\eta} \geq 0$), extracted from the mutual orientation matrix $\mathbf{R}_e(\boldsymbol{\sigma}_b, \boldsymbol{\zeta})\mathbf{R}_{e,d}^T$.

If $n + 4 = 6$, the aerial manipulator is non-redundant, thus \mathbf{J}_ζ is square and the pseudo-inverse in (16) coincides with the inverse. On the other hand, if $n + 4 > 6$ the aerial manipulator is kinematically redundant and the redundant DOFs can be exploited to fulfill secondary tasks by resorting to a task-priority approach.^{28,34}

Since in this paper lower-priority tasks are not used, the so-called internal motions, i.e., motions of the structure that do not change the end-effector position and orientation, must be stabilized. According to [35], this can be achieved by adding a damping term projected onto the null space of \mathbf{J}_ζ , i.e.,

$$\begin{aligned} \ddot{\boldsymbol{\zeta}}_r = & \mathbf{J}_\zeta^\dagger(\boldsymbol{\sigma}_b, \boldsymbol{\zeta}) (\dot{\mathbf{v}}_{e,d} + \mathbf{K}_v(\mathbf{v}_{e,d} - \mathbf{v}_e) + \mathbf{K}_p \mathbf{e}) - \\ & \mathbf{J}_\zeta^\dagger(\boldsymbol{\sigma}_b, \boldsymbol{\zeta}) \left(\dot{\mathbf{J}}_\zeta(\boldsymbol{\sigma}_b, \boldsymbol{\zeta}) \dot{\boldsymbol{\zeta}} + \mathbf{J}_\sigma(\boldsymbol{\sigma}_b, \boldsymbol{\zeta}) \ddot{\boldsymbol{\sigma}}_b + \dot{\mathbf{J}}_\sigma(\boldsymbol{\sigma}_b, \boldsymbol{\zeta}) \dot{\boldsymbol{\sigma}}_b \right) - \\ & \mathbf{N}(\mathbf{J}_\zeta) \left(k_N \mathbf{I}_{n+4} + \dot{\mathbf{N}} \right) \dot{\boldsymbol{\zeta}}, \end{aligned} \quad (19)$$

where $\mathbf{N}(\mathbf{J}_\zeta)$ is a projector onto the null space of the Jacobian \mathbf{J}_ζ ; a possible choice is $\mathbf{N}(\mathbf{J}_\zeta) = \mathbf{I}_{n+4} - \mathbf{J}_\zeta^\dagger \mathbf{J}_\zeta$. More details can be found in Appendix A.

3.2. Motion Control

Once $\boldsymbol{\zeta}_r$ and its time derivatives are computed by the inverse kinematics algorithm (16), they are fed to the low-level motion controller in charge of achieving the desired motion. Two kinds of hierarchical motion controllers have been compared: a model-based controller and a PID controller.

3.3. Model-based controller

This is a hierarchical inner-outer loop control scheme. The outer control loop is designed to track the assigned position and yaw angle for the vehicle, by introducing a virtual control vector aimed at linearizing the position dynamics. Then, by using the relation between the force vector \mathbf{u}_f and the quadrotor attitude, a reference value for the roll and pitch angles is devised and used to feed an attitude controller (inner loop).

In order to design the control law, it is worth rewriting the system model (11) as

$$\overline{\mathbf{M}}(\boldsymbol{\xi}) \ddot{\boldsymbol{\xi}} + \mathbf{C}(\dot{\boldsymbol{\xi}}, \boldsymbol{\xi}) \dot{\boldsymbol{\xi}} + \mathbf{g}(\boldsymbol{\xi}) + \Delta \mathbf{M}(\boldsymbol{\xi}) \ddot{\boldsymbol{\xi}} + \mathbf{d}(\boldsymbol{\xi}, \dot{\boldsymbol{\xi}}) = \mathbf{u}, \quad (20)$$

where the matrix $\overline{\mathbf{M}}$ is obtained by setting to zero the second and third columns of $\mathbf{M}_{p\phi}$ in (14), namely

$$\overline{\mathbf{M}}(\boldsymbol{\xi}) = \begin{bmatrix} \mathbf{M}_{pp} & \overline{\mathbf{M}}_{p\phi} & \mathbf{M}_{pq} \\ \mathbf{M}_{p\phi}^\top & \mathbf{M}_{\phi\phi} & \mathbf{M}_{\phi q} \\ \mathbf{M}_{pq}^\top & \mathbf{M}_{\phi q}^\top & \mathbf{M}_{qq} \end{bmatrix}, \quad (21)$$

with $\overline{\mathbf{M}}_{p\phi} = [\mathbf{m}_{p\phi} \mathbf{0}_3 \mathbf{0}_3]$, where $\mathbf{m}_{p\phi}$ denotes the first column of $\mathbf{M}_{p\phi}$, and $\mathbf{0}_3$ is the (3×1) null vector.

In order to globally linearize the closed-loop dynamics, the following adaptive control law can be considered

$$\mathbf{u} = \overline{\mathbf{M}}(\boldsymbol{\xi}) \boldsymbol{\alpha} + \mathbf{C}(\boldsymbol{\xi}, \dot{\boldsymbol{\xi}}) \dot{\boldsymbol{\xi}} + \mathbf{g}(\boldsymbol{\xi}) + \mathbf{r}(\boldsymbol{\xi}, \dot{\boldsymbol{\xi}}), \quad (22)$$

where the auxiliary input $\boldsymbol{\alpha}$ can be partitioned according to (12) as $\boldsymbol{\alpha} = [\boldsymbol{\alpha}_p^T \ \boldsymbol{\alpha}_\phi^T \ \boldsymbol{\alpha}_q^T]^T$, with $\boldsymbol{\alpha}_\phi = [\alpha_\psi \ \alpha_\theta \ \alpha_\varphi]^T$. The term $\mathbf{r} = [\mathbf{r}_p^T \ \mathbf{r}_\phi^T \ \mathbf{r}_q^T]^T$ is an adaptive term aimed at compensating both the disturbance \mathbf{d} and the term $\Delta\mathbf{M}$ in (20).

The auxiliary controls $\boldsymbol{\alpha}_q$, $\boldsymbol{\alpha}_p$ and α_ψ can be chosen as

$$\boldsymbol{\alpha}_q = \ddot{\mathbf{q}}_r + \mathbf{K}_{q,V}(\dot{\mathbf{q}}_r - \dot{\mathbf{q}}) + \mathbf{K}_{q,P}(\mathbf{q}_r - \mathbf{q}), \quad (23)$$

$$\boldsymbol{\alpha}_p = \ddot{\mathbf{p}}_{b,r} + \mathbf{K}_{p,V}(\dot{\mathbf{p}}_{b,r} - \dot{\mathbf{p}}_b) + \mathbf{K}_{p,P}(\mathbf{p}_{b,r} - \mathbf{p}_b), \quad (24)$$

$$\alpha_\psi = \ddot{\psi}_{b,r} + k_{\psi,V}(\dot{\psi}_{b,r} - \dot{\psi}_b) + k_{\psi,P}(\psi_{b,r} - \psi_b), \quad (25)$$

where $\mathbf{K}_{*,V}, \mathbf{K}_{*,P}$ ($* = \{q, p\}$) are symmetric positive definite matrices and $k_{\psi,V}, k_{\psi,P}$ are positive scalar gains.

3.3.1. Quadrotor position controller. On the basis of (22), the following expression of \mathbf{u}_f can be derived

$$\mathbf{u}_f = \mathbf{M}_{pp}\boldsymbol{\alpha}_p + \mathbf{m}_{p\phi}\alpha_\psi + \mathbf{M}_{pq}\boldsymbol{\alpha}_q + \mathbf{C}_p\dot{\boldsymbol{\xi}} + \mathbf{g}_p + \mathbf{r}_p, \quad (26)$$

where the function dependencies have been dropped for notation compactness.

Remark 3.1. In (22) matrix $\overline{\mathbf{M}}$ is used in lieu of \mathbf{M} , otherwise it would not have been possible to compute \mathbf{u}_f , since it depends on α_φ and α_θ , which, in turn, require the reference values for roll and pitch angles, not available at this stage.

In view of (12), \mathbf{u}_f depends on the attitude of the quadrotor via the relation

$$\mathbf{u}_f = \mathbf{h}(f_z, \boldsymbol{\sigma}_b) \Rightarrow \begin{bmatrix} u_{f,x} \\ u_{f,y} \\ u_{f,z} \end{bmatrix} = \begin{bmatrix} (c_{\psi_b} s_{\theta_b} c_{\varphi_b} + s_{\psi_b} s_{\varphi_b}) f_z \\ (s_{\psi_b} s_{\theta_b} c_{\varphi_b} - c_{\psi_b} s_{\varphi_b}) f_z \\ c_{\theta_b} c_{\varphi_b} f_z \end{bmatrix}, \quad (27)$$

therefore, the total thrust, f_z , and reference trajectories for the roll and pitch angles to be fed to the inner loop can be computed as

$$f_z = \|\mathbf{u}_f\|, \quad (28)$$

$$\theta_{b,r} = \arctan\left(\frac{u_{f,x} c_{\psi_{b,r}} + u_{f,y} s_{\psi_{b,r}}}{u_{f,z}}\right), \quad (29)$$

$$\varphi_{b,r} = \arcsin\left(\frac{u_{f,x} s_{\psi_{b,r}} - u_{f,y} c_{\psi_{b,r}}}{\|\mathbf{u}_f\|}\right). \quad (30)$$

Remark 3.2. From (27) it could be noted that (29)–(30) are not well defined if

- $\|\mathbf{u}_f\|$ vanishes: it can happen only if $f_z = 0$;
- $\theta_r = \pm\pi/2$ or $\phi_r = \pm\pi/2$.

It is assumed that f_z is always non-null, while both θ_r and ϕ_r are defined in $(-\pi/2 \ \pi/2)$. These are reasonable assumptions for quadrotor vehicles not involved in acrobatic maneuvers.

3.3.2. Quadrotor attitude control. Once the reference values for roll and pitch angles have been computed, the control inputs α_θ and α_φ can be obtained via

$$\alpha_\theta = \ddot{\theta}_{b,r} + k_{\theta,V}(\dot{\theta}_{b,r} - \dot{\theta}_b) + k_{\theta,P}(\theta_{b,r} - \theta_b), \quad (31)$$

$$\alpha_\varphi = \ddot{\varphi}_{b,r} + k_{\varphi,V}(\dot{\varphi}_{b,r} - \dot{\varphi}_b) + k_{\varphi,P}(\varphi_{b,r} - \varphi_b), \quad (32)$$

where $k_{\theta,P}$, $k_{\theta,V}$, $k_{\varphi,P}$ and $k_{\varphi,V}$ are positive scalar gains. It is worth noticing that (31) and (32) require the first and second time derivative of θ_r and φ_r , that can not be directly obtained from (27), but only via numerical differentiation. Since in a practical scenario θ_r and φ_r are likely to be affected by noise, the reference velocities and accelerations must be realistically computed by using robust-to-noise filters. More in detail, in this paper, the time-varying filter proposed in [36] has been designed in order to compute both the first and second time-derivatives of θ_r and φ_r . By using this approach, the derivative estimation is based on truncated Taylor series expansion of the signal and is quite accurate for short time intervals. Moreover, such a filter allows a quasi-instantaneous estimation and results to be robust to Gaussian noise.³⁶

Finally, \mathbf{u}_μ can be computed as

$$\mathbf{u}_\mu = \mathbf{M}_{p\phi}^T \boldsymbol{\alpha}_p + \mathbf{M}_{\phi\phi} \boldsymbol{\alpha}_\phi + \mathbf{M}_{\phi q} \boldsymbol{\alpha}_q + \mathbf{C}_\phi \dot{\boldsymbol{\xi}} + \mathbf{g}_\phi + \mathbf{r}_\phi. \quad (33)$$

From (12), the vehicle torques can be computed as

$$\boldsymbol{\mu}_b^b = \mathbf{R}_b^T(\boldsymbol{\phi}_b) \mathbf{T}^{-T}(\boldsymbol{\phi}_b) \mathbf{u}_\mu. \quad (34)$$

3.3.3. Computation of quadrotor inputs. Once f_z and $\boldsymbol{\mu}_b^b$ have been computed, the four actuation forces of the vehicle rotors can be easily obtained by inverting (13), i.e.,

$$\mathbf{f} = \boldsymbol{\Gamma}^{-1} \begin{bmatrix} f_z \\ \boldsymbol{\mu}_b^b \end{bmatrix}. \quad (35)$$

3.3.4. Manipulator control. Finally, the torques acting on the manipulator joints can be computed as

$$\mathbf{u}_q = \mathbf{M}_{p\phi}^T \boldsymbol{\alpha}_p + \mathbf{M}_{\phi q}^T \boldsymbol{\alpha}_\phi + \mathbf{M}_{qq} \boldsymbol{\alpha}_q + \mathbf{C}_q \dot{\boldsymbol{\xi}} + \mathbf{g}_q + \mathbf{r}_q. \quad (36)$$

3.4. PID controller

Often an accurate knowledge of the inertial matrix and Coriolis terms requires a time consuming identification procedure and, thus, a simpler control law can be adopted. In order to test the proposed controller, a model-free approach is considered in the following, where the knowledge of the dynamic parameters is not required. More in detail, regarding to the UAV position control, a standard PID law is adopted in lieu of (26)

$$\mathbf{u}_f^{PID} = \mathbf{K}_{p,P}^{PID} (\mathbf{p}_{b,r} - \mathbf{p}_b) + \mathbf{K}_{p,D}^{PID} (\dot{\mathbf{p}}_{b,r} - \dot{\mathbf{p}}_b) + \mathbf{K}_{p,I}^{PID} \int_0^t (\mathbf{p}_{b,r}(\tau) - \mathbf{p}_b(\tau)) d\tau, \quad (37)$$

whose output is fed to equation (27) in order to determine the reference values for the roll and pitch angles as well as the total thrust. Regarding to the attitude control, in order to confer more robustness to the system, a cascade control is implemented, where the outer loop controls the orientation angles, while the inner loop is aimed at controlling the rapid changing angular velocities and reads the output of outer loop controller as setpoint. More in detail, the outer loop is a PI controller while the inner one is a PID, tuned in such a way that the inner loop is faster than the outer. Such attitude control scheme is inherited by [29].

$$\dot{\boldsymbol{\phi}}_r^{PI} = \mathbf{K}_{\phi,P}^{PI} (\boldsymbol{\phi}_{b,r} - \boldsymbol{\phi}_b) + \mathbf{K}_{\phi,I}^{PI} \int_0^t (\boldsymbol{\phi}_{b,r}(\tau) - \boldsymbol{\phi}_b(\tau)) d\tau, \quad (38)$$

$$\mathbf{u}_\mu^{PID} = \mathbf{K}_{\phi,P}^{PID} (\dot{\boldsymbol{\phi}}_r^{PI} - \dot{\boldsymbol{\phi}}_b) - \mathbf{K}_{\phi,D}^{PID} \ddot{\boldsymbol{\phi}}_b + \mathbf{K}_{\phi,I}^{PID} \int_0^t (\dot{\boldsymbol{\phi}}_r^{PI}(\tau) - \dot{\boldsymbol{\phi}}_b(\tau)) d\tau, \quad (39)$$

Regarding to the arm, again a standard PID law is designed i.e

$$\mathbf{u}_q^{PID} = \mathbf{K}_{q,P}^{PID}(\mathbf{q}_r - \mathbf{q}) + \mathbf{K}_{q,D}^{PID}(\dot{\mathbf{q}}_r - \dot{\mathbf{q}}) + \mathbf{K}_{q,I}^{PID} \int_0^t (\mathbf{q}_r(\tau) - \mathbf{q}(\tau)) d\tau. \quad (40)$$

3.5. Discussion.

In the previous section two different control approaches have been proposed: a model-based adaptive controller and a cascade PID regulator. PIDs refer to standard techniques which do not require the knowledge of the dynamics of the controlled system, and, as consequence, practical implementation turns to be easy even in terms of computational burden. PID controllers are able to track arbitrary trajectories with acceptable tracking errors, eventually zero thanks to the integral action, if the desired controlled variable has a steady-state phase. On the contrary, model-based techniques require an accurate knowledge of the system's dynamic model; in principle, the dynamic is linearized by exploiting both state feedback and dynamic model knowledge, with the effect of reducing the system to a double integrator: at this point, it is possible to impose the desired behavior to the overall control system. Obviously, model-based controllers require a non-negligible identification effort although they result to be more accurate and robust in the presence of external disturbances. Since the perfect knowledge of the dynamics is an ideal condition, an adaptive term is adopted to counteract the effects of model uncertainties and, of course, external disturbances.

4. Uncertainties Estimation

By folding the control law (22) in (20), and by considering that $\overline{\mathbf{M}} = \mathbf{M} - \Delta\mathbf{M}$, the closed-loop dynamics becomes

$$\ddot{\boldsymbol{\xi}} = \boldsymbol{\alpha} - \mathbf{M}^{-1}(\boldsymbol{\xi}) (\Delta\mathbf{M}\boldsymbol{\alpha} + \mathbf{d} - \mathbf{r}). \quad (41)$$

Thus, the compensation term \mathbf{r} has to take into account not only the modeling uncertainties, \mathbf{d} , but also the perturbation given by the implementation of the control law, namely the use of $\overline{\mathbf{M}}$ in lieu of \mathbf{M} in (22).

Let us rearrange (41) as

$$\ddot{\boldsymbol{\xi}} = \boldsymbol{\alpha} - \boldsymbol{\delta} + \widehat{\boldsymbol{\delta}} = \boldsymbol{\alpha} - \widetilde{\boldsymbol{\delta}}, \quad (42)$$

where

$$\boldsymbol{\delta} = \mathbf{M}^{-1}(\boldsymbol{\xi}) (\Delta\mathbf{M}\boldsymbol{\alpha} + \mathbf{d}), \quad \widehat{\boldsymbol{\delta}} = \mathbf{M}^{-1}(\boldsymbol{\xi})\mathbf{r}. \quad (43)$$

A good approximations of the term $\boldsymbol{\delta}$ can be obtained by resorting to a parametric model, i.e.,

$$\boldsymbol{\delta} = \boldsymbol{\Lambda}(\boldsymbol{\xi}, \dot{\boldsymbol{\xi}})\boldsymbol{\chi} + \boldsymbol{\varsigma}, \quad (44)$$

where $\boldsymbol{\chi}$ is a $(p \times 1)$ vector of constant parameters, $\boldsymbol{\Lambda}$ is a $(n + 6 \times p)$ regressor matrix and $\boldsymbol{\varsigma}$ is the $(n + 6 \times 1)$ interpolation error. Of course, not all the uncertainties can be rigorously characterized by a linear-in-the-parameters structure; however, this modeling assumption is not too restrictive, since it has been demonstrated that it is valid for a wide class of functions.³⁷ The elements of the regressor matrix can be chosen as Radial Basis Functions (RBFs)

$$\lambda_{i,h}(\boldsymbol{\xi}, \dot{\boldsymbol{\xi}}) = \exp\left(-\frac{\|\mathbf{z} - \mathbf{c}_{i,h}\|^2}{2\sigma^2}\right), \quad \mathbf{z} = \begin{bmatrix} \boldsymbol{\xi}^T & \dot{\boldsymbol{\xi}}^T \end{bmatrix}^T,$$

where $\mathbf{c}_{i,h}$ and σ are the centroid and the width of the function, respectively. According to the Universal Interpolation Theorem,³⁸ any continuous function can be approximated (in the \mathcal{L}_p -norm sense, $p \in [1, \infty)$) by a RBF-network with suitably chosen centroids and a common width, provided that the basis functions $\lambda_{i,h}(\boldsymbol{\xi}, \dot{\boldsymbol{\xi}})$ are continuous, bounded, integrable and with non-null integral over \mathbb{R}^{3n} . Since $\boldsymbol{\delta}$ can be reasonably assumed continuous and the RBFs satisfy the conditions of the theorem, there exists a RBF network (44), i.e., a suitable sets of weights, widths and centroids, capable of approximating $\boldsymbol{\delta}$ to any degree of accuracy. Thus, the interpolation error $\boldsymbol{\varsigma}$ in (44) can be reasonably assumed norm bounded,

$$\|\boldsymbol{\varsigma}(t)\| \leq \bar{\varsigma}, \quad \forall t \geq 0. \quad (45)$$

An estimate,

$$\hat{\boldsymbol{\delta}} = \boldsymbol{\Lambda}(\boldsymbol{\xi}, \dot{\boldsymbol{\xi}})\hat{\boldsymbol{\chi}}, \quad (46)$$

of $\boldsymbol{\delta}$ can be obtained by integrating the following update law for the unknown parameters $\boldsymbol{\chi}$

$$\dot{\hat{\boldsymbol{\chi}}} = \frac{1}{\beta} \boldsymbol{\Lambda}^T \mathbf{B}^T \mathbf{Q} \begin{bmatrix} \tilde{\boldsymbol{\xi}} \\ \tilde{\dot{\boldsymbol{\xi}}} \end{bmatrix}, \quad (47)$$

where β is a positive scalar gain, \mathbf{Q} is a symmetric and positive definite matrix, $\mathbf{B} = [\mathbf{O}_{6+n} \ \mathbf{I}_{6+n}]^T$ and $\tilde{\boldsymbol{\xi}} = \boldsymbol{\xi}_r - \boldsymbol{\xi}$ is the inner loop error.

From (43), then, \mathbf{r} can be easily obtained as $\mathbf{r} = \mathbf{M}(\boldsymbol{\xi})\hat{\boldsymbol{\delta}}$.

5. Stability Analysis

To prove the stability of the closed-loop system, let us consider the convergence of both the kinematic control outer loop and the motion control inner loop.

5.1. Inner loop

By considering (42), the following dynamics for the inner loop error $\tilde{\boldsymbol{\xi}}$ can be derived

$$\ddot{\tilde{\boldsymbol{\xi}}} = -\boldsymbol{\Omega}_V \dot{\tilde{\boldsymbol{\xi}}} - \boldsymbol{\Omega}_P \tilde{\boldsymbol{\xi}} + \tilde{\boldsymbol{\delta}}, \quad (48)$$

where $(* = V, P)$

$$\boldsymbol{\Omega}_* = \begin{bmatrix} -\mathbf{K}_{p,*} & \mathbf{O}_3 & \mathbf{O}_3 \\ \mathbf{O}_3 & -\mathbf{K}_{\phi,*} & \mathbf{O}_3 \\ \mathbf{O}_n & \mathbf{O}_n & -\mathbf{K}_{q,*} \end{bmatrix},$$

with $\mathbf{K}_{\phi,*} = \text{diag}\{k_{\psi,*}, k_{\theta,*}, k_{\varphi,*}\}$. Let us rearrange (48) in the state space form, by considering $\tilde{\mathbf{z}} = [\tilde{\mathbf{z}}_1^T \ \tilde{\mathbf{z}}_2^T]^T = [\tilde{\boldsymbol{\xi}}^T \ \dot{\tilde{\boldsymbol{\xi}}}^T]^T$ and assuming $\boldsymbol{\varsigma} = \mathbf{0}$, as

$$\dot{\tilde{\mathbf{z}}} = \boldsymbol{\Omega} \tilde{\mathbf{z}} + \mathbf{B} \tilde{\boldsymbol{\delta}} = \boldsymbol{\Omega} \tilde{\mathbf{z}} + \mathbf{B} \boldsymbol{\Lambda} \tilde{\boldsymbol{\chi}}, \quad (49)$$

where $\tilde{\boldsymbol{\chi}} = \boldsymbol{\chi} - \hat{\boldsymbol{\chi}}$ and $\boldsymbol{\Omega} = \begin{bmatrix} \mathbf{O}_{6+n} & \mathbf{I}_{6+n} \\ -\boldsymbol{\Omega}_V & -\boldsymbol{\Omega}_P \end{bmatrix}$.

The following theorem can be stated for the inner loop error convergence.

Theorem 1. *Given the system (49) and the update law (47), for any set of positive definite matrix gains $\mathbf{K}_{p,*}$, $\mathbf{K}_{\phi,*}$ and $\mathbf{K}_{q,*}$ ($* = V, P$), the equilibrium $\tilde{\mathbf{z}} = \mathbf{0}$ is globally asymptotically stable, while the parameter error $\tilde{\boldsymbol{\chi}}$ is bounded.*

Proof. In order to analyze the stability of the system (49), the following Lyapunov function candidate can be considered

$$V_i = \frac{1}{2} \tilde{\mathbf{z}}^T \mathbf{Q} \tilde{\mathbf{z}} + \frac{\beta}{2} \tilde{\boldsymbol{\chi}}^T \tilde{\boldsymbol{\chi}}, \quad (50)$$

where \mathbf{Q} is the symmetric positive definite matrix defined in (47). The time derivative of V_i yields

$$\dot{V}_i = -\tilde{\mathbf{z}}^T \mathbf{P}_z \tilde{\mathbf{z}} + \tilde{\mathbf{z}}^T \mathbf{Q} \mathbf{B} \boldsymbol{\Lambda} \tilde{\boldsymbol{\chi}} + \beta \dot{\tilde{\boldsymbol{\chi}}}^T \tilde{\boldsymbol{\chi}}, \quad (51)$$

where \mathbf{P}_z is the symmetric and positive definite solution to the Lyapunov equation

$$\mathbf{P}_z = -(\mathbf{Q} \boldsymbol{\Omega} + \boldsymbol{\Omega}^T \mathbf{Q}), \quad (52)$$

that always exists, since, if $\mathbf{K}_{p,*}$, $\mathbf{K}_{\phi,*}$ and $\mathbf{K}_{q,*}$ ($*$ = V, P) are positive definite, $\boldsymbol{\Omega}$ is Hurwitz. Under the assumption of parameter $\boldsymbol{\chi}$ constant and by considering the update law (47), \dot{V}_i can be rewritten as

$$\dot{V}_i = -\tilde{\mathbf{z}}^T \mathbf{P}_z \tilde{\mathbf{z}} + \tilde{\mathbf{z}}^T \mathbf{Q} \mathbf{B} \boldsymbol{\Lambda} \tilde{\boldsymbol{\chi}} - \beta \dot{\tilde{\boldsymbol{\chi}}}^T \tilde{\boldsymbol{\chi}} = -\tilde{\mathbf{z}}^T \mathbf{P}_z \tilde{\mathbf{z}}. \quad (53)$$

Since \mathbf{P}_z is positive definite, \dot{V}_i is negative semi-definite; this guarantees the boundedness of $\tilde{\mathbf{z}}$ and $\tilde{\boldsymbol{\chi}}$. By invoking the Barbalat's lemma,³⁹ it can be recognized that $\dot{V}_i \rightarrow 0$, which implies the global asymptotic convergence to $\mathbf{0}$ of $\tilde{\mathbf{z}}$ as $t \rightarrow \infty$, while, as usual in direct adaptive control,⁴⁰ $\tilde{\boldsymbol{\chi}}$ is only guaranteed to be uniformly bounded. \square

Remark 5.1. The global convergence of $\tilde{\mathbf{z}}$ is ensured only when the pitch angles, both the reference and actual one, are different from $\pm h\pi/2$ for any integer h .

Corollary 1. *In the presence of the persistency of excitation (PE) condition,³⁹ i.e., if there exist positive scalars κ_1, κ_2, T such that*

$$\kappa_1 \mathbf{I}_p \geq \int_t^{t+T} \boldsymbol{\Lambda}^T(\boldsymbol{\xi}(\sigma), \dot{\boldsymbol{\xi}}(\sigma)) \boldsymbol{\Lambda}(\boldsymbol{\xi}(\sigma), \dot{\boldsymbol{\xi}}(\sigma)) d\sigma \geq \kappa_2 \mathbf{I}_p, \quad (54)$$

both $\tilde{\mathbf{z}}$ and $\tilde{\boldsymbol{\chi}}$ are exponentially convergent to zero.

Proof. The proof can be found in Appendix B. \square

In general $\boldsymbol{\varsigma} \neq \mathbf{0}$ and, thus, the inner loop error dynamics becomes

$$\dot{\tilde{\mathbf{z}}} = \boldsymbol{\Omega} \tilde{\mathbf{z}} + \mathbf{B} (\boldsymbol{\Lambda} \tilde{\boldsymbol{\chi}} + \boldsymbol{\varsigma}). \quad (55)$$

It worth pointing out that the system (55) can be viewed as the nominal system (49) with a non-vanishing perturbation term, $\mathbf{B}\boldsymbol{\varsigma}$, which, in turn, is norm bounded since $\|\mathbf{B}\| = 1$ and (45) holds; thus, from Lemma 5.2 in [39] it can be recognized that both $\tilde{\mathbf{z}}$ and $\tilde{\boldsymbol{\chi}}$ are norm bounded as well.

If persistency of excitation cannot be met, in order to ensure the boundedness of $\tilde{\boldsymbol{\chi}}$ even in the presence of bounded interpolation error, the update law (47) can be modified by adopting the so-called *projection operator*⁴¹ i.e.

$$\dot{\hat{\boldsymbol{\chi}}} = Pr \left[\hat{\boldsymbol{\chi}}, \frac{1}{\beta} \boldsymbol{\Lambda}^T \mathbf{B}^T \mathbf{Q} \mathbf{z} \right], \quad (56)$$

where the projection operator, $Pr[\mathbf{a}_1, \mathbf{a}_2]$, is given by

$$Pr[\mathbf{a}_1, \mathbf{a}_2] = \begin{cases} \mathbf{a}_2 & \text{if } \|\mathbf{a}_1\| < \varrho \text{ or if} \\ & \|\mathbf{a}_1\| = \varrho, \mathbf{a}_1^\top \mathbf{a}_2 \leq \mathbf{0} \\ \mathbf{a}_2 - \frac{\mathbf{a}_1^\top \mathbf{a}_2}{\|\mathbf{a}_1\|^2} \mathbf{a}_1 & \text{otherwise.} \end{cases}$$

In other words, the projection operator ensures that the estimate $\hat{\chi}$ never leaves the hypersphere

$$\mathcal{S} = \{\hat{\chi} : \|\hat{\chi}\| \leq \varrho\},$$

and thus, $\tilde{\chi}$ keeps uniformly bounded in the presence of uncertainties as well. Now, the system (55) can be seen as the nominal linear system

$$\dot{\tilde{\mathbf{z}}} = \mathbf{\Omega} \tilde{\mathbf{z}}, \quad (57)$$

which is exponentially stable, since $\mathbf{\Omega}$ is Hurwitz, plus a bounded perturbation term

$$\|\mathbf{B}(\mathbf{\Lambda} \tilde{\chi} + \varsigma)\| \leq \|\mathbf{\Lambda}\| \|\tilde{\chi}\| + \bar{\varsigma}, \quad (58)$$

where $\mathbf{\Lambda}$ is norm-bounded being a matrix of bounded functions. Again, by recalling Lemma 5.2 in [39], it can be stated that $\tilde{\mathbf{z}}$ is norm bounded.

Remark 5.2. For nonlinear systems, the *a priori* verification of the PE condition is usually very difficult. However, for the special case of regressor matrices constructed from RBF approximators, there are some interesting results showing that the PE condition can be met for particular kind of periodic or recurrent trajectories \mathbf{z} passing through the neighborhood of the RBF centroids.⁴²

5.2. Kinematic control outer loop

Under the assumption of perfect acceleration tracking (i.e. $\ddot{\zeta} = \ddot{\zeta}_r$), by folding (16) in (15), the following relation holds

$$\dot{\mathbf{v}}_{e,d} - \dot{\mathbf{v}}_e = -\mathbf{K}_v (\mathbf{v}_{e,d} - \mathbf{v}_e) - \mathbf{K}_p \mathbf{e}. \quad (59)$$

Let us consider the following inverse kinematics error

$$\boldsymbol{\varepsilon} = \begin{bmatrix} \boldsymbol{\varepsilon}_P \\ \boldsymbol{\varepsilon}_O \end{bmatrix}, \quad \boldsymbol{\varepsilon}_P = \begin{bmatrix} \mathbf{e}_P \\ \dot{\mathbf{e}}_P \end{bmatrix}, \quad \boldsymbol{\varepsilon}_O = \begin{bmatrix} \mathbf{e}_O \\ \tilde{\boldsymbol{\omega}}_e \end{bmatrix}, \quad (60)$$

where \mathbf{e}_P and \mathbf{e}_O are defined in (18), while $\tilde{\boldsymbol{\omega}}_e = \boldsymbol{\omega}_{e,d} - \boldsymbol{\omega}_e$.

Theorem 2. *Given the system (59), there exists a set of positive definite matrix gains \mathbf{K}_p and \mathbf{K}_v , chosen as in (17) with $k_{v,O} > 1/2$, such that the equilibrium $\boldsymbol{\varepsilon} = \mathbf{0}$ is exponentially stable.*

Proof. To prove the asymptotic stability of the equilibrium $\boldsymbol{\varepsilon} = \mathbf{0}$, let us consider the following candidate Lyapunov function⁴³

$$V_o = (\tilde{\boldsymbol{\varepsilon}} + \tilde{\boldsymbol{\omega}}_e)^\top (\tilde{\boldsymbol{\varepsilon}} + \tilde{\boldsymbol{\omega}}_e) + 2k_{v,O} (1 - \tilde{\eta})^2 + \tilde{\boldsymbol{\omega}}_e^\top \tilde{\boldsymbol{\omega}}_e + (2k_{v,O} - 1) \tilde{\boldsymbol{\varepsilon}}^\top \tilde{\boldsymbol{\varepsilon}} + \boldsymbol{\varepsilon}_P^\top \mathbf{Q}_P \boldsymbol{\varepsilon}_P, \quad (61)$$

where \mathbf{Q}_P is a symmetric and positive definite matrix, $\tilde{\mathcal{Q}} = \{\tilde{\eta}, \tilde{\boldsymbol{\varepsilon}}\}$ is the unit quaternion extracted from the mutual orientation matrix $\mathbf{R}_e \mathbf{R}_{e,d}^\top$, whose vector part $\tilde{\boldsymbol{\varepsilon}}$, by virtue of (18), represents the orientation error \mathbf{e}_O .

By considering the so-called *quaternion propagation*³⁰

$$\begin{aligned}\dot{\tilde{\eta}} &= -\frac{1}{2}\tilde{\boldsymbol{\epsilon}}^T\tilde{\boldsymbol{\omega}}_e, \\ \dot{\tilde{\boldsymbol{\epsilon}}} &= \frac{1}{2}(\tilde{\eta}\mathbf{I}_3 - \mathbf{S}(\tilde{\boldsymbol{\epsilon}}))\tilde{\boldsymbol{\omega}}_e,\end{aligned}\quad (62)$$

the time derivative of V_o is given by

$$\begin{aligned}\dot{V}_o &= -2\mathbf{e}_O^T\mathbf{K}_{p,O}\mathbf{e}_O - 4\tilde{\boldsymbol{\omega}}_e^T\mathbf{K}_{p,O}\mathbf{e}_O - 4k_{v,o}\tilde{\boldsymbol{\omega}}_e^T\tilde{\boldsymbol{\omega}}_e + \\ &\quad \eta\tilde{\boldsymbol{\omega}}_e^T\tilde{\boldsymbol{\omega}}_e + \boldsymbol{\varepsilon}_P^T(\mathbf{Q}_P\mathbf{A}_P + \mathbf{A}_P^T\mathbf{Q}_P)\boldsymbol{\varepsilon}_P,\end{aligned}\quad (63)$$

where

$$\mathbf{A}_P = \begin{bmatrix} \mathbf{O}_3 & \mathbf{I}_3 \\ -\mathbf{K}_{p,P} & -\mathbf{K}_{v,P} \end{bmatrix},$$

and $\mathbf{K}_{*,O}$ and $\mathbf{K}_{*,P}$ ($* = v, p$) are defined in (17). Since \mathbf{A}_P is Hurwitz, there always exists a matrix \mathbf{P}_P , symmetric and positive definite, solution to the Lyapunov equation

$$\mathbf{Q}_P\mathbf{A}_P + \mathbf{A}_P^T\mathbf{Q}_P = -\mathbf{P}_P.$$

Hence, the function \dot{V}_o can be upper bounded as

$$\begin{aligned}\dot{V}_o &\leq -2\lambda_m(\mathbf{K}_{p,O})\|\mathbf{e}_O\|^2 - (4k_{v,O} - 1)\|\tilde{\boldsymbol{\omega}}_e\|^2 \\ &\quad + 4\lambda_M(\mathbf{K}_{p,O})\|\tilde{\boldsymbol{\omega}}_e\|\|\mathbf{e}_O\| - \lambda_m(\mathbf{P}_P)\|\boldsymbol{\varepsilon}_P\|^2 \\ &\leq -\begin{bmatrix} \|\mathbf{e}_O\| \\ \|\tilde{\boldsymbol{\omega}}_e\| \end{bmatrix}^T \boldsymbol{\Xi} \begin{bmatrix} \|\mathbf{e}_O\| \\ \|\tilde{\boldsymbol{\omega}}_e\| \end{bmatrix} - \lambda_m(\mathbf{P}_P)\|\boldsymbol{\varepsilon}_P\|^2,\end{aligned}\quad (64)$$

with

$$\boldsymbol{\Xi} = \begin{bmatrix} 2\lambda_m(\mathbf{K}_{p,O}) & -2\lambda_M(\mathbf{K}_{p,O}) \\ -2\lambda_M(\mathbf{K}_{p,O}) & 4k_{v,O} - 1 \end{bmatrix},$$

and $\lambda_m(\cdot)$ and $\lambda_M(\cdot)$ representing the minimum and maximum eigenvalue of a matrix. If the following inequality holds

$$k_{v,O} > \frac{1}{4} + \frac{\lambda_M^2(\mathbf{K}_{p,O})}{2\lambda_m(\mathbf{K}_{p,O})}, \quad (65)$$

matrix $\boldsymbol{\Xi}$ is positive definite, therefore, by recalling that $k_{v,O} > 1/2$, a sufficient condition on $k_{v,O}$ can be stated as

$$k_{v,O} > \max\left\{\frac{1}{2}, \frac{1}{4} + \frac{\lambda_M^2(\mathbf{K}_{p,O})}{2\lambda_m(\mathbf{K}_{p,O})}\right\}. \quad (66)$$

\dot{V}_o can be upper bounded as

$$\dot{V}_o \leq -\lambda_m(\boldsymbol{\Xi})\|\boldsymbol{\varepsilon}_O\|^2 - \lambda_m(\mathbf{P}_P)\|\boldsymbol{\varepsilon}_P\|^2 \leq -\lambda_\varepsilon\|\boldsymbol{\varepsilon}\|^2, \quad (67)$$

where $\lambda_\varepsilon = \min\{\lambda_m(\boldsymbol{\Xi}), \lambda_m(\mathbf{P}_P)\}$.

Thus, since \dot{V}_o is negative definite the error $\boldsymbol{\varepsilon}$ is asymptotically convergent to zero.

Moreover, the convergence is exponential, since, from the fact that a unit quaternion with scalar part $0 \leq \tilde{\eta} \leq 1$ is chosen (see Section 3.1), it holds

$$\|\tilde{\epsilon}\|^2 = 1 - \tilde{\eta}^2 \geq 1 - \tilde{\eta}, \quad (68)$$

thus, V_o can be bounded as follows

$$c_m \|\epsilon\|^2 \leq V_o \leq c_M \|\epsilon\|^2, \quad (69)$$

with

$$c_m = \min\{(2k_{v,O} - 1), 1, \lambda_m(\mathbf{Q}_P)\},$$

$$c_M = \max\{(4k_{v,O} + 1), \lambda_M(\mathbf{Q}_P)\}.$$

□

Remark 5.3. Theorem 2 does not hold globally because of the limitation in the unit quaternion domain due to the choice $0 \leq \tilde{\eta} \leq 1$; in practice, this is not a true limitation since it allows to represent all the orientations.

5.3. Two-loop dynamics

The convergence properties of the two-loop system, namely (49) and (59), is stated by following Theorem.

Theorem 3. *Under the assumption of perfect acceleration tracking, in the presence of the PE condition (54) and in the absence of the interpolation error ($\varsigma = \mathbf{0}$), on the basis of Corollary 1 and Theorem 2, ϵ , $\tilde{\mathbf{z}}$ and $\tilde{\chi}$ are exponentially convergent to zero.*

Proof. See Appendix B. □

In practice, the inner loop cannot guarantee instantaneous perfect tracking of the desired acceleration, therefore by considering the error $\ddot{\zeta} = \ddot{\zeta}_r - \ddot{\zeta}$, the outer loop error dynamics (59) becomes

$$\dot{\mathbf{v}}_{e,d} - \dot{\mathbf{v}}_e = -\mathbf{K}_v(\mathbf{v}_{e,d} - \mathbf{v}_e) - \mathbf{K}_p \mathbf{e} + \mathbf{J}_\zeta \ddot{\zeta}. \quad (70)$$

The perturbation term $\mathbf{J}_\zeta \ddot{\zeta}$ can be upper bounded as

$$\begin{aligned} \|\mathbf{J}_\zeta \ddot{\zeta}\| &\leq \|\mathbf{J}_\zeta\| \|\ddot{\zeta}\| \leq \|\mathbf{J}_\zeta\| \|\dot{\tilde{\mathbf{z}}}\| \leq \|\mathbf{J}_\zeta\| (\|\Omega\| \|\tilde{\mathbf{z}}\| + \|\tilde{\delta}\|) \\ &\leq \|\mathbf{J}_\zeta\| \|\Omega\| \|\tilde{\mathbf{z}}\| + \|\mathbf{J}_\zeta\| \|\Lambda\| \|\tilde{\chi}\|. \end{aligned} \quad (71)$$

The norm $\|\mathbf{J}_\zeta\|$ in (71) is bounded since all the manipulator joints are revolute joints, therefore the first term in (71) can be viewed as a vanishing perturbation.³⁹ In the case $\varsigma = \mathbf{0}$, the second term in (71) is, at least, bounded, since, from Theorem 1, $\tilde{\chi}$ is at least bounded, while, as already specified, Λ is norm-bounded. Therefore, the convergence properties of the two-loop system, described by (49) and (70), are stated by the following Theorem.

Theorem 4. *Let the PE condition (54) be fulfilled and $\varsigma = \mathbf{0}$, then the equilibrium $\tilde{\mathbf{v}} = [\tilde{\mathbf{z}}^T \ \epsilon^T]^T = \mathbf{0}$ of the two-loop system (49)-(70) is asymptotically stable.*

Proof. See Appendix B. □

When $\varsigma \neq \mathbf{0}$, by recalling (58), the upper bound on $\|\mathbf{J}_\zeta \ddot{\zeta}\|$ becomes

$$\|\mathbf{J}_\zeta \ddot{\zeta}\| \leq \|\mathbf{J}_\zeta\| \|\Omega\| \|\tilde{\mathbf{z}}\| + \|\mathbf{J}_\zeta\| (\|\Lambda\| \|\tilde{\chi}\| + \bar{\varsigma}). \quad (72)$$

In the presence of bounded interpolation error, it has been already proven in Section 5.1 that $\tilde{\chi}$ is norm bounded as well, even if the PE condition cannot be met. Therefore, the following corollary can be stated.

Corollary 2. In the presence of bounded interpolation error ς and bounded estimation error $\tilde{\chi}$, the error $\tilde{\nu}$ of the two-loop system is norm-bounded as well.

Proof. See Appendix B. □

6. Simulation Results

The effectiveness of the proposed algorithm has been tested in simulation by considering the model of an eight rotors aircrafts in coaxial configuration equipped with a 6-DOFs robotic arm⁴⁴ with all revolute joints, depicted in Fig. 1. The Denavit-Hartenberg parameters of the manipulator are reported in Table I. Such a model reproduces the experimental setup developed within the EU-funded project ARCAS (Aerial Robotics Cooperative Assembly System),⁴⁵ and has been validated on the real system.

Table I . Denavit-Hartenberg parameters of the 6 DOF manipulator.

Joint	d [mm]	ϑ [rad]	a [mm]	α [rad]
1	0	ϑ_1	-7	$\pi/2$
2	0	ϑ_2	246.8	0
3	0	$\vartheta_3 + \pi/2$	0	$\pi/2$
4	110.5	ϑ_4	0	$-\pi/2$
5	0	ϑ_5	0	$\pi/2$
6	111.3	ϑ_6	0	0

The dynamic model of the whole system has been developed in the Matlab/SimMechanics environment. The masses and inertias have been estimated via CAD tools: the aerial vehicle mass has been assumed as $m_b = 4.493$ kg while the inertia matrix is $I_b = \text{diag}\{0.177, 0.177, 0.334\}$ kgm²; as for the manipulator, a total weight of 750 g has been assumed, with the following link masses $m_{l_1} = 156$ g, $m_{l_2} = 225$ g, $m_{l_3} = 78$ g, $m_{l_4} = 56$ g, $m_{l_5} = 76$ g, $m_{l_6} = 134$ g, while the moments of inertia of each link about its center of mass are reported in Table II.

Table II . Moments of inertia of each link [kgm²].

Link	I_{xx}	I_{yy}	I_{zz}	I_{xy}	I_{xz}	I_{yz}
1	4.4e-5	7.4e-5	6.0e-5	1.1e-6	1.3e-6	4.2e-8
2	3.2e-4	2.3e-3	2.1e-3	8.4e-6	-2.0e-6	-6.3e-7
3	2.7e-5	2.8e-5	2.3e-5	2.1e-9	2.5e-6	-1.1e-10
4	2.0e-5	1.1e-5	1.7e-5	1.7e-9	-4.5e-10	-6.2e-8
5	2.3e-5	2.4e-5	2.2e-5	-5.9e-10	1.1e-6	-3.3e-10
6	1.5e-4	9.0e-5	1.2e-4	1.8e-7	9.9e-7	-2.7e-6

A realistic scenario has been simulated by assuming that only vehicle position, orientation and joint positions are available as feedback, while the velocity measurements have been numerically obtained via a suitable first-order filter with a time constant of 0.03 s. Moreover, zero mean normally distributed measurement noise, with standard deviation 10^{-3} m for the vehicle's position, $5 \cdot 10^{-3}$ rad for vehicle's orientation and $5 \cdot 10^{-4}$ rad for joints positions, has been added. The controller has been digitally implemented: all feedback data are updated at a sampling frequency of 200 Hz, while the model has been simulated at a frequency rate of 1 kHz. The frequency rate of 200 Hz is compatible with the commonly used equipment for indoor aerial manipulation. Moreover, the robustness of the proposed algorithm to disturbances and model uncertainties has been tested since relevant uncertainties and disturbances have been considered:

Table III . Model-based adaptive controller parameters.

Gain	Value	Gain	Value
$\mathbf{K}_{p,P}$	$12 \cdot \mathbf{I}_3$	$\mathbf{K}_{p,V}$	$8 \cdot \mathbf{I}_3$
$\mathbf{K}_{q,P}$	$150 \cdot \mathbf{I}_6$	$\mathbf{K}_{q,V}$	$50 \cdot \mathbf{I}_6$
$k_{\psi,P}$	6.4	$k_{\psi,V}$	3
$k_{\theta,P}$	5	$k_{\theta,V}$	5
$k_{\phi,P}$	5	$k_{\phi,V}$	5
\mathbf{K}_p	$\text{diag}\{9 \cdot \mathbf{I}_3, 8 \cdot \mathbf{I}_3\}$	\mathbf{K}_v	$\text{diag}\{8 \cdot \mathbf{I}_3, 7 \cdot \mathbf{I}_3\}$
β	5	\mathbf{Q}	$\text{diag}\{\mathbf{O}_{12}, 25 \cdot \mathbf{I}_3, 8 \cdot \mathbf{I}_3, 100 \cdot \mathbf{I}_6\}$
k_N	0.6		

Table IV . PID controller parameters.

Gain	Value	Gain	Value	Gain	Value
$\mathbf{K}_{p,P}^{PID}$	$\text{diag}\{150, 150, 200\}$	$\mathbf{K}_{p,D}^{PID}$	$30 \cdot \mathbf{I}_3$	$\mathbf{K}_{p,I}^{PID}$	$1.5 \cdot \mathbf{I}_3$
$\mathbf{K}_{\phi,P}^{PID}$	$30 \cdot \mathbf{I}_3$	$\mathbf{K}_{\phi,D}^{PID}$	$5 \cdot \mathbf{I}_3$	$\mathbf{K}_{\phi,I}^{PID}$	$1.2 \cdot \mathbf{I}_3$
$\mathbf{K}_{\phi,P}^{PI}$	$15 \cdot \mathbf{I}_3$			$\mathbf{K}_{\phi,I}^{PI}$	$0.75 \cdot \mathbf{I}_3$
$\mathbf{K}_{q,P}^{PID}$	$\text{diag}\{1.1, 0.9, 0.6, 0.4, 0.5, 0.2\}$			$\mathbf{K}_{q,D}^{PID}$	$0.05 \cdot \mathbf{I}_6$
\mathbf{K}_p	$\text{diag}\{0.9 \cdot \mathbf{I}_3, 1.6 \cdot \mathbf{I}_3\}$			$\mathbf{K}_{q,I}^{PID}$	$0.05 \cdot \mathbf{I}_6$
\mathbf{K}_v	$\text{diag}\{0.8 \cdot \mathbf{I}_3, 1.1 \cdot \mathbf{I}_3\}$			k_N	0.6

- in control laws (26), (33) and (36), the compensation of the Centrifugal and Coriolis terms, \mathbf{C} , has been neglected;
- an aerodynamic disturbance, acting on the vehicle vessel from time $t_w = 20$ s, has been considered and modeled as⁴⁶

$$\mathbf{d}(t) = \mathbf{K}_w \|\mathbf{v}_b\| \sin\left(\frac{2\pi}{T_w}(t - t_w)\right) \mathbf{v}_b, \quad (73)$$

where $\mathbf{K}_w = \text{diag}\{10 \cdot \mathbf{I}_3, \mathbf{I}_3\}$ and $T_w = 10$ s;

- viscous friction, $\boldsymbol{\tau}_f$, acting on the joints, has been modeled but not considered in the control design, as

$$\boldsymbol{\tau}_f = -\mathbf{F} \|\dot{\mathbf{q}}\| \dot{\mathbf{q}}, \quad (74)$$

where $\mathbf{F} = \text{diag}\{0.02 \cdot \mathbf{I}_6\}$ is the matrix of friction coefficients.

The end-effector is commanded to track an helical trajectory having radius of 1 m and pitch of $\pi/3$ (see Fig. 3), by rotating, at same time, the end-effector frame of $\pi/4$ around yaw and roll axes. At the end of the path a hovering phase of 5 s is commanded.

A comparison between the proposed model-based and the PID controller has been conducted and, in order to present a fair comparison, the PID control gains have been tuned to achieve the best control performance and to ensure control efforts of the same order of magnitude of the model-based ones; the gains of the two control laws are reported in Tables III and IV, respectively.

Figure 3 reports the end-effector desired trajectory together with the trajectories obtained by using the model-based adaptive law (red line) and the PID law (yellow line), while Fig. 4 shows the norm of the end-effector position (Fig. 4(a)) and orientation (Fig. 4(b)) errors. As can be seen, the adaptive controller allows to track the desired end effector trajectory in a more accurate way during the whole simulation; in particular, in the presence of the disturbance (73) (i.e., starting from 20 s), it keeps the error close to zero with a peak value of about 1 cm, while the error of the PID controller becomes much

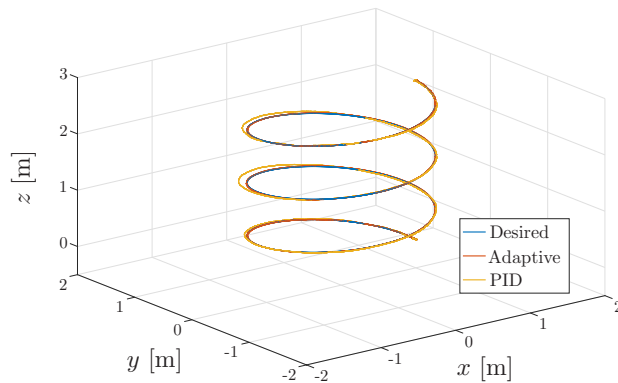


Fig. 3. Comparison between the end-effector desired trajectory (blue) and the actual ones, obtained with the model-based adaptive controller (red) and the PID controller (yellow).

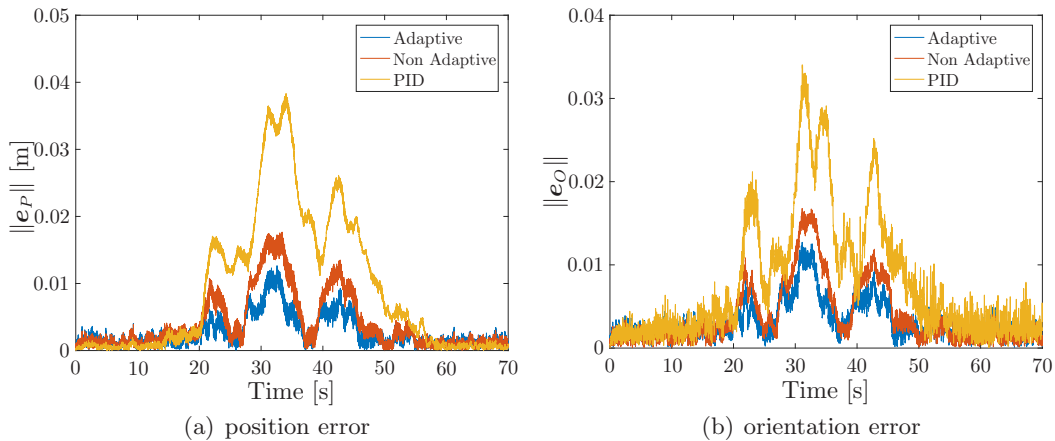


Fig. 4. End-effector pose error norm. Comparison between model-based adaptive (blue), non-adaptive (red) and standard PID (yellow) controllers.

larger with a peak value of about 4 cm. Also regarding the orientation error, the model-based schemes allow to achieve better results with respect to the PID scheme. Regarding the comparison between the adaptive and non-adaptive model based controllers, it can be viewed that the adaptive one still performs well but the differences are smaller and the errors are practically indistinguishable in the absence of aerodynamic disturbs: this is mainly due to the presence of the external loop, which improves the overall tracking capabilities even if the inner-loop is not so accurate as the adaptive one.

Figure 5 depicts the norm of the low-level motion control errors obtained by comparing the three different approaches: the standard PID (37)–(40), the proposed model-based law without the compensation term \mathbf{r} , and the model-based law with the adaptive compensation \mathbf{r} . It can be noticed that, regarding the UAV position and the joint position, the PID performance is quite poor with respect to the model-based one, especially in the presence of the disturbance term (73), while regarding to the UAV attitude, the PID performance is quite similar to the model-based one, but it is characterized by a larger noise, due to the velocity loop. The adaptive term allows to have better tracking both for the UAV and for the manipulator joints.

Figures 6-7, report the vehicle thrusts and the manipulator torques, respectively. The thrusts and joint torques concerning the non-adaptive model-based control are not reported since there are not appreciable difference with respect to the adaptive ones. It is

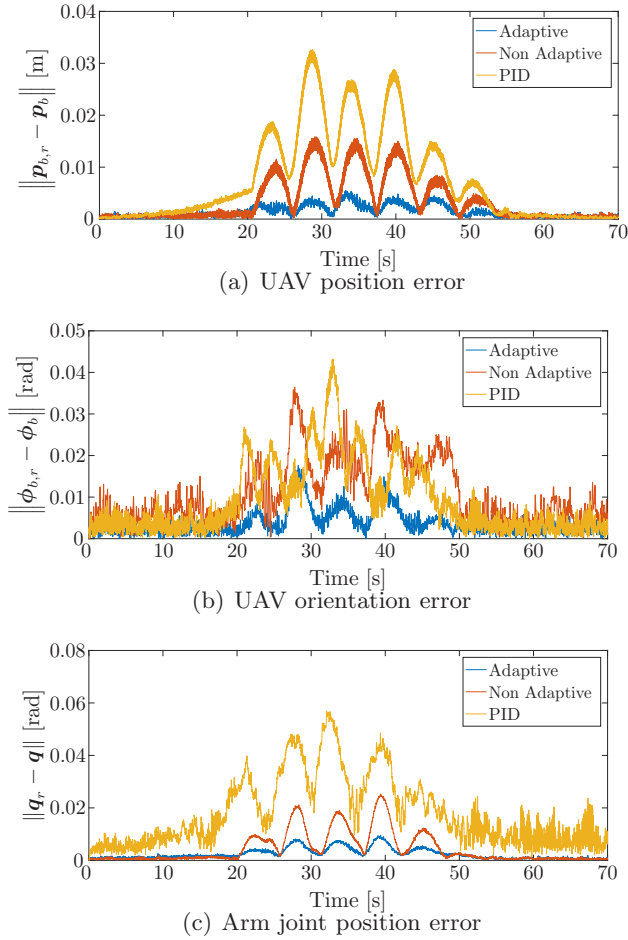


Fig. 5. Comparison among the low-level motion control errors norms by adopting the model-based controller with (blue) and without (red) the adaptive compensation as well as the standard PID (yellow).

worth pointing out that the vehicle thrusts are compatible with the modeled hardware, while the manipulator torques can be easily achieved by commercial servos.

Finally, Fig. 8 presents the aerodynamic disturbance \mathbf{d} acting on the vehicle vessel, experienced during the simulation with the adaptive model-based controller. For the sake of brevity, the disturbances experienced with different controllers are not reported, since they are very similar to that reported in Fig. 8. Based on (73), the disturbance depends on the vehicle velocity, thus it becomes almost zero after about 55 s, while the peak value is about 5.8 N along x and y axes and 1.6 N along z axis.

It can be concluded that the model-based control results to be robust to non-negligible external forces (of about 6 N), and it performs better than a PID, commonly adopted in commercial vehicles. Moreover, the adaptive controller achieves better tracking at low level with respect to the model-based, but at end-effector level its effect is less evident, due to the presence of the outer loop.

7. Conclusions

In this paper, a hierarchical motion control scheme has been proposed for an aerial manipulator, composed of a multirotor aerial vehicle equipped with a multi-DOFs robotic arm. First, on the basis of the desired pose of the manipulator end-effector, a closed-loop inverse kinematics algorithm computes the references for the vehicle position, the vehicle yaw angle and the manipulator joints. Then, a cascade controller, with an adaptive

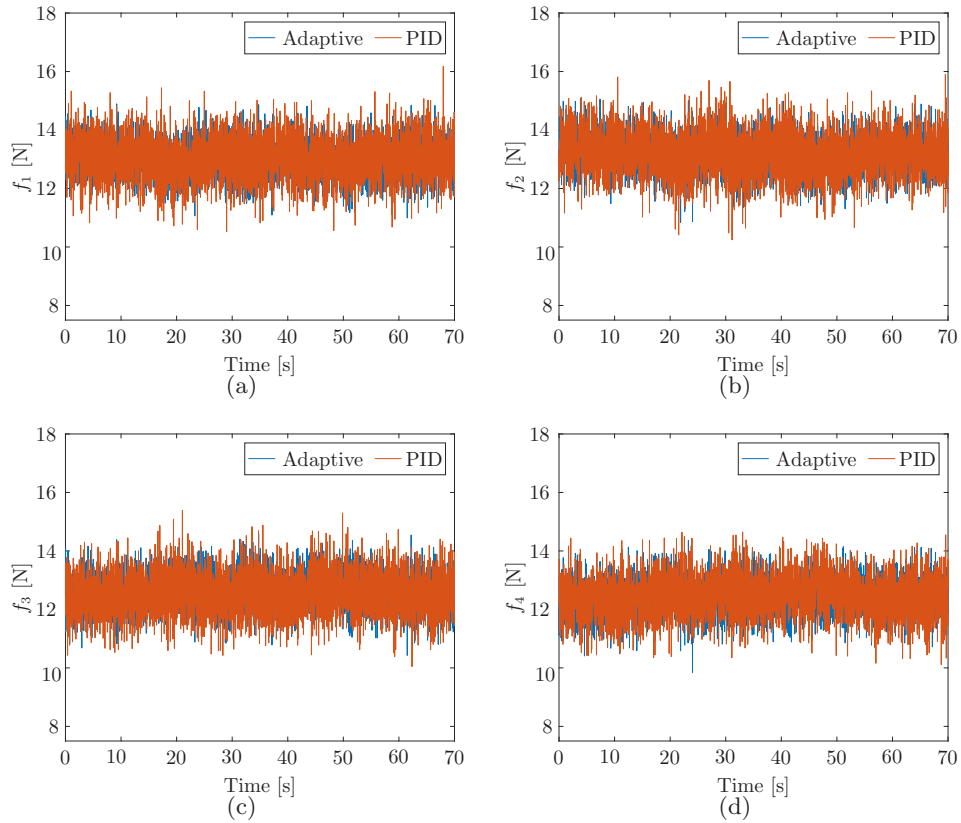


Fig. 6. Control effort: thrust of the coaxial rotors for the adaptive (blue) and PID (red) controller

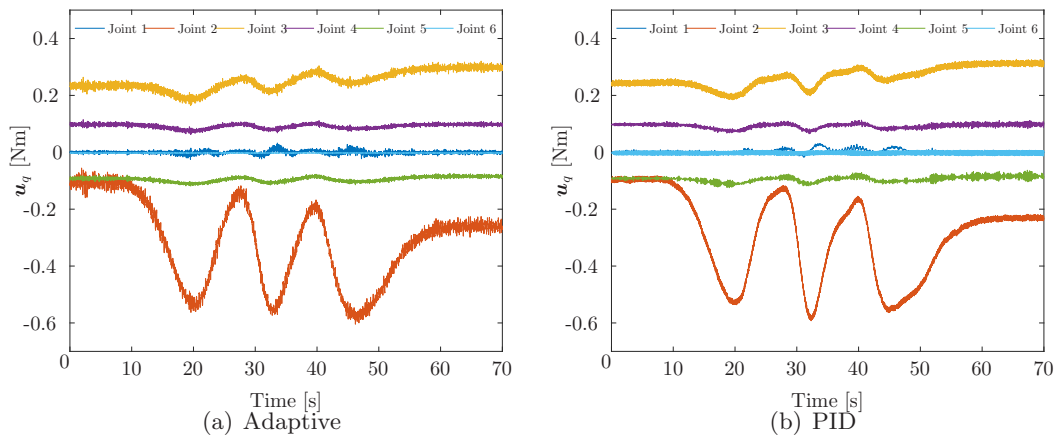


Fig. 7. Control effort: manipulator joint torques.

term designed to counteract uncertainties, ensures tracking of the desired trajectories. The stability of the proposed control scheme has been theoretically proven. A realistic simulation case study has been developed, in which the algorithm is tested in the presence of digital implementation of the controller, measurement noise and disturbances. On the basis of the simulation results, the adaptive compensation, which is needed to ensure convergence, provides slightly better performance with respect to the model-based

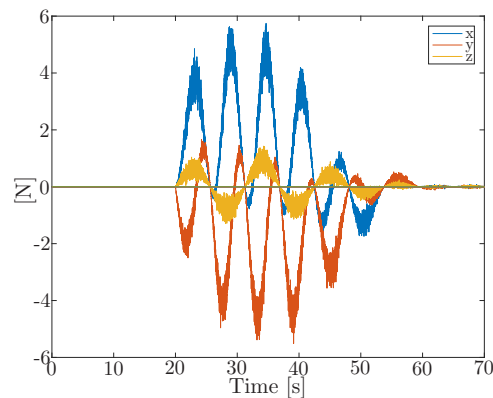


Fig. 8. Aerodynamic disturbs acting on the vehicle vessel.

controller without adaption, that, in turn, is still superior to simple linear (e.g., PID) control approaches.

Acknowledgements

The research leading to these results has received funding from the European Commission's 7th Framework Program under grant agreement No.287617 (IP project ARCAS - Aerial Robotics Cooperative Assembly system) and from the European Commission's Horizon 2020 Program under grant agreement No. 644271 (IP project AEROARMS - AERial RObotic system integrating multiple ARMS and advanced manipulation capabilities for inspection and maintenance).

References

1. Doitsidis, L., Weiss, S., Renzaglia, A., Kosmatopoulos, E., Siegwart, R., Scaramuzza, D., Achtelik, M.: Optimal surveillance coverage for teams of micro aerial vehicles in gps-denied environments using onboard vision. *Autonomous Robots* (2012)
2. Maza, I., Kondak, K., Bernard, M., Ollero, A.: Multi-UAV cooperation and control for load transportation and deployment. *Journal of Intelligent and Robotic Systems* **57**, 417–449 (2010)
3. Maza, I., Ollero, A.: Autonomous transportation and deployment with aerial robots for search and rescue missions. *Journal of Field Robotics* **28**(6), 914931 (2011)
4. Merino, L., Caballero, F., Martinez-de-Dios, J., Maza, I., Ollero, A.: An unmanned aircraft system for automatic forest fire monitoring and measurement. *Journal of Intelligent and Robotic Systems* **65**(1), 533–548 (2012)
5. How, J., Bethke, B., Frank, A., Dale, D., Vian, J.: Real-time indoor autonomous vehicle test environment. *IEEE Control Systems Magazine* **28**(2), 51–64 (2008)
6. Civita, M.L., Papageorgiou, G., Messner, W., Kanade, T.: Design and flight testing of an H_∞ controller for a robotic helicopter. *Journal of Guidance, Control, and Dynamics* **29**(2), 485–494 (2006)
7. Kim, H., Shim, D.: A flight control system for aerial robots: Algorithms and experiments. *Control Engineering Practice* **11**(2), 1389–1400 (2003)
8. Ahanda, J.J.B.M., Mbede, J.B., Melingui, A., Essimbi, B.: Robust adaptive control for robot manipulators: Support vector regression-based command filtered adaptive backstepping approach. *Robotica* **36**(4), 516–534 (2018)
9. Madani, T., Benallegue, A.: Backstepping sliding-mode control applied to a miniature quadrotor flying robot. In: *Proc. of the 32nd Annual Conference of the IEEE Industrial Electronics Society*, pp. 700–705 (2006)
10. Palunko, I., Fierro, R.: Adaptive control of a quadrotor with dynamic changes in the center of gravity. In: *Proc. of the 18th IFAC World Congress*, pp. 2626–2631 (2011)
11. Antonelli, G., Cataldi, E., Arrichiello, F., Giordano, P.R., Chiaverini, S., Franchi, A.: Adaptive trajectory tracking for quadrotor mavs in presence of parameter uncertainties and external disturbances. *IEEE Transactions on Control Systems Technology* **26**(1), 248–254 (2018)
12. Kendoul, F., Fantoni, I., Lozano, R.: Asymptotic stability of hierarchical inner-outer loop-based flight controllers. In: *Proc. of the 17th IFAC World Congress*, pp. 1741–1746 (2008)

13. Pounds, P., Bersak, D., Dollar, A.: Grasping from the air: Hovering capture and load stability. In: Proc. of IEEE Int. Conf. on Robotics and Automation (ICRA), pp. 2491–2498 (2011)
14. Mellinger, D., Lindsey, Q., Shomin, M., Kumar, V.: Design, modelling, estimation and control for aerial grasping and manipulation. In: Proc. of IEEE/RSJ International Conference on Intelligent Robots and Systems, pp. 2668–2673 (2011)
15. Ruggiero, F., Lippiello, V., Ollero, A.: Aerial manipulation: A literature review. *IEEE Robotics and Automation Letters* **3**(3), 1957–1964 (2018)
16. Kondak, K., Krieger, K., Albu Schaeffer, A., Ollero, A.: Closed-loop behavior of an autonomous helicopter equipped with a robotic arm for aerial manipulation tasks. *International Journal of Advanced Robotic Systems* **10**, 1–9 (2013)
17. Huber, F., Kondak, K., Krieger, K., Sommer, D., Schwarzbach, M., Laiacker, M., Kossyk, I., Parusel, S., Haddadin, S., Albu-Schaeffer, A.: First analysis and experiments in aerial manipulation using fully actuated redundant robot arm. In: Intelligent Robots and Systems (IROS), 2013 IEEE/RSJ International Conference on, pp. 3452–3457 (2013)
18. Kondak, K., Huber, F., Schwarzbach, M., Laiacker, M., Sommer, D., Bejar, M., Ollero, A.: Aerial manipulation robot composed of an autonomous helicopter and a 7 degrees of freedom industrial manipulator. In: Robotics and Automation (ICRA), 2014 IEEE International Conference on, pp. 2107–2112 (2014)
19. Antonelli, G., Cataldi, E.: Adaptive control of arm-equipped quadrotors. theory and simulations. In: Proceedings of 22th Mediterranean Conference on Control and Automation (2014)
20. Fumagalli, M., Naldi, R., Macchelli, A., Forte, F., Keemink, A., Stramigioli, S., Carloni, R., Marconi, L.: Developing an aerial manipulator prototype: Physical interaction with the environment. *IEEE Robotics Automation Magazine* **21**(3), 41–50 (2014)
21. Kim, S., Choi, S., Kim, H.: Aerial manipulation using a quadrotor with a two dof robotic arm. In: Intelligent Robots and Systems (IROS), 2013 IEEE/RSJ International Conference on, pp. 4990–4995 (2013)
22. Orsag, M., Korpela, C., Oh, P.: Modeling and control of MM-UAV: Mobile manipulating unmanned aerial vehicle. *Journal of Intelligent and Robotic Systems* **69**, 227–240 (2013)
23. Lippiello, V., Ruggiero, F.: Cartesian impedance control of uav with a robotic arm. In: Proc. of 10th International IFAC Symposium on Robot Control (SYROCO), pp. 704–709 (2012)
24. Ryll, M., Muscio, G., Pierri, F., Cataldi, E., Antonelli, G., Caccavale, F., Franchi, A.: 6d physical interaction with a fully actuated aerial robot. In: Robotics and Automation (ICRA), 2017 IEEE International Conference on, pp. 5190–5195. IEEE (2017)
25. Arleo, G., Caccavale, F., Muscio, G., Pierri, F.: Control of quadrotor aerial vehicles equipped with a robotic arm. In: Proc. of 21th Mediterranean Conference on Control and Automation, pp. 1174–1180 (2013)
26. Kannan, S., Bezzaoucha, S., Guzman, S.Q., Dentler, J., Olivares-Mendez, M.A., Voos, H.: Hierarchical control of aerial manipulation vehicle. In: AIP Conference Proceedings, vol. 1798, pp. 1–7. AIP Publishing (2017)
27. Caccavale, F., Giglio, G., Muscio, G., Pierri, F.: Adaptive control for UAVs equipped with a robotic arm. In: Proceedings of the 19th World Congress The International Federation of Automatic Control (IFAC), pp. 11,049–11,054 (2014)
28. Baizid, K., Giglio, G., Pierri, F., Trujillo, M.A., Antonelli, G., Caccavale, F., Viguria, A., Chiaverini, S., Ollero, A.: Behavioral control of unmanned aerial vehicle manipulator systems. *Autonomous Robots* **41**(5), 1203–1220 (2017)
29. Ren, J., Liu, D.X., Li, K., Liu, J., Feng, Y., Lin, X.: Cascade pid controller for quadrotor. 2016 IEEE International Conference on Information and Automation (ICIA) pp. 120–124 (2016)
30. Siciliano, B., Sciacvico, L., Villani, L., Oriolo, G.: *Robotics – Modelling, Planning and Control*. Springer, London, UK (2009)
31. Nonami, K., Kendoul, F., Suzuki, S., Wang, W.: *Atonomous Flying Robots, Unmanned Aerial Vehicles and Micro Aerial Vehicles*. Springer, London, UK (2010)
32. Caccavale, F., Chiaverini, S., Siciliano, B.: Second-order kinematic control of robot manipulators with jacobian damped least-squares inverse: Theory and experiments. *IEEE/ASME Transactions on Mechatronics* **2**, 188–194 (1997)
33. Chiaverini, S., Siciliano, B.: The unit quaternion: A useful tool for inverse kinematics of robot manipulators. *Systems Analysis Modelling Simulation* **35**, 45–60 (1999)
34. Muscio, G., Pierri, F., Trujillo, M., Cataldi, E., Antonelli, G., Caccavale, F., Viguria, A., Chiaverini, S., Ollero, A.: Coordinated control of aerial robotic manipulators: Theory and experiments. *IEEE Transactions on Control Systems Technology* (2017)
35. Hsu, P., Hauser, J., Sastry, S.: Dynamic control of redundant manipulators. In: Proc. of IEEE International Conference on Robotics and Automation (ICRA), pp. 183–187 vol.1 (1988)
36. Reger, J., Ramírez, H.S., Fliess, M.: On non-asymptotic observation of nonlinear systems. In: Proceedings of the 44th IEEE Conference on Decision and Control, pp. 4219–4224. IEEE (2005)
37. Caccavale, F., Marino, A., Muscio, G., Pierri, F.: Discrete-time framework for fault diagnosis in robotic manipulators. *IEEE Transactions on Control Systems Technology* **21**(5), 1858–1873 (2013)
38. Park, J., Sandberg, I.: Universal approximation using radial-basis-function networks. *Neural Computation* **3**, 246–257 (1991)

39. Khalil, H.: Nonlinear Systems (2nd ed.). Prentice Hall, Upper Saddle River, NJ (1996)
40. Aström, K., Wittenmark, B.: Adaptive control (2nd ed.). Addison-Wesley (1995)
41. Ioannou, P., Sun, J.: Robust Adaptive Control. Prentice Hall, Upper Saddle River, NJ (1996)
42. Wang, C., Hill, D.J.: Learning from neural control. Neural Networks, IEEE Transactions on **17**(1), 130–146 (2006)
43. Tayebi, A., McGilvray, S.: Attitude stabilization of a vtol quadrotor aircraft. Control Systems Technology, IEEE Transactions on **14**(3), 562–571 (2006)
44. Cano, R., Pérez, C., Pruaño, F., Ollero, A., Heredia, G.: Mechanical design of a 6-DOF aerial manipulator for assembling bar structures using UAVs. In: 2nd RED-UAS 2013 Workshop on Research, Education and Development of Unmanned Aerial Systems (2013)
45. ARCAS - Aerial Robotics Cooperative Assembly System. URL <http://www.arcas-project.eu>
46. Castaldi, P., Mimmo, N., Naldi, R., Marconi, L.: Robust trajectory tracking for underactuated vtol aerial vehicles: Extended for adaptive disturbance compensation. In: Proc. of 19-th IFAC World Congress, vol. 19, pp. 3184–3189 (2014)
47. Sontag, E.: A remark on the converging-input converging-state property. Automatic Control, IEEE Transactions on **48**(2), 313–314 (2003)

Appendix A: Internal motion stabilization

Let us consider the projection of $\dot{\zeta}$ onto the null space of \mathbf{J}_ζ

$$\dot{\zeta}_N = \mathbf{N}(\mathbf{J}_\zeta)\dot{\zeta}. \quad (\text{A1})$$

Its time derivative, $\ddot{\zeta}_N$ can be rewritten as

$$\ddot{\zeta}_N = \dot{\mathbf{N}}\dot{\zeta} + \mathbf{N}\ddot{\zeta}, \quad (\text{A2})$$

where the dependencies of \mathbf{N} and $\dot{\mathbf{N}}$ have been dropped for notation compactness. By folding (19) in (A2), and by resorting to the following properties of each projector onto the null space

- $\mathbf{N}(\mathbf{J}_\zeta)\mathbf{J}_\zeta^\dagger = \mathbf{O}_{n+4 \times 6}$;
- \mathbf{N} is idempotent, namely $\mathbf{N}\mathbf{N} = \mathbf{N}$,

the following relation holds

$$\ddot{\zeta}_N = \dot{\mathbf{N}}\dot{\zeta} - \mathbf{N}\dot{\mathbf{N}}\dot{\zeta} - k_N\mathbf{N}\dot{\zeta}. \quad (\text{A3})$$

In order to prove the convergence to zero of $\dot{\zeta}_N$, let us consider the candidate Lyapunov function

$$V_N = \frac{1}{2}\dot{\zeta}_N^\top \dot{\zeta}_N, \quad (\text{A4})$$

and its time derivative, given by

$$\dot{V}_N = \dot{\zeta}_N^\top \ddot{\zeta}_N = \dot{\zeta}_N^\top \mathbf{N}^\top \dot{\mathbf{N}}\dot{\zeta} - \dot{\zeta}_N^\top \mathbf{N}^\top \mathbf{N}\dot{\mathbf{N}}\dot{\zeta} - k_N\dot{\zeta}_N^\top \mathbf{N}^\top \mathbf{N}\dot{\zeta}.$$

Since each null projector matrix is symmetric and idempotent, after few steps it yields

$$\dot{V}_N = -k_N\dot{\zeta}_N^\top \dot{\zeta}_N, \quad (\text{A5})$$

which is negative definite, therefore $\dot{\zeta}_N$ converges to $\mathbf{0}$ exponentially. This proves that equation (19) allows to stabilize the internal motion.

Appendix B: Proofs

Proof of Corollary 1

In order to prove the Corollary 1, by considering the state space equation of the system (49), with the parameters' estimation error having the following dynamics

$$\dot{\tilde{\chi}} = -\dot{\hat{\chi}} = -\frac{1}{\beta} \mathbf{\Lambda}^T \mathbf{B}^T \mathbf{Q} \begin{bmatrix} \tilde{\xi} \\ \dot{\tilde{\xi}} \end{bmatrix}, \quad (\text{A6})$$

and the augmented state $\bar{\mathbf{z}} = [\tilde{\mathbf{z}}^T \tilde{\chi}^T]^T$, the closed-loop dynamics of the inner loop can be rewritten as the following time-varying system

$$\begin{cases} \dot{\bar{\mathbf{z}}} = \mathbf{A}(t) \bar{\mathbf{z}} \\ \mathbf{y} = \mathbf{L} \bar{\mathbf{z}}, \end{cases} \quad (\text{A7})$$

with

$$\mathbf{A}(t) = \begin{bmatrix} \mathbf{\Omega} & \mathbf{B} \mathbf{\Lambda} \\ -\frac{1}{\beta} \mathbf{\Lambda}^T \mathbf{B}^T \mathbf{Q} & \mathbf{O}_p \end{bmatrix},$$

and

$$\mathbf{L} = \begin{bmatrix} \sqrt{\mathbf{P}_z} & \mathbf{O} \\ \mathbf{O} & \mathbf{O} \end{bmatrix},$$

where \mathbf{P}_z is the solution to the Lyapunov equation (52). The Lyapunov function (50) can be bounded as follows

$$\frac{1}{2} \min\{\lambda_m(\mathbf{Q}), \beta\} \|\bar{\mathbf{z}}\|^2 \leq V_i \leq \frac{1}{2} \max\{\lambda_M(\mathbf{Q}), \beta\} \|\bar{\mathbf{z}}\|^2, \quad (\text{A8})$$

while the time derivative \dot{V}_i can be upper bounded as

$$\dot{V}_i \leq -\bar{\mathbf{z}}^T \mathbf{L}^T \mathbf{L} \bar{\mathbf{z}}. \quad (\text{A9})$$

By resorting to Theorem 4.5 in [39], it can be argued, by looking at (A8)–(A9), that V_i verifies the first two conditions imposed by the Theorem and, thus, to prove the exponential stability, it is sufficient to show that the condition

$$\int_t^{t+\delta t} \dot{V}_i(\sigma) d\sigma \leq -\lambda V_i(t), \quad \lambda > 0,$$

is met as well. To this aim, it is worth considering the evolution of V_i on the time interval $[t, t + \delta t]$ for some $\delta t > 0$

$$\int_t^{t+\delta t} \dot{V}_i(\sigma) d\sigma = - \int_t^{t+\delta t} \bar{\mathbf{z}}^T \mathbf{L}^T \mathbf{L} \bar{\mathbf{z}} d\sigma = -\bar{\mathbf{z}}^T \mathbf{W}(t, t + \delta t) \bar{\mathbf{z}}, \quad (\text{A10})$$

where $\mathbf{W}(t, t + \delta t)$ is the observability Gramian of the pair (\mathbf{A}, \mathbf{L}) . The pair (\mathbf{A}, \mathbf{L}) is uniformly observable, i.e. $\mathbf{W}(t, t + \delta t) \geq k_w \mathbf{I}$ ($k_w > 0$), if and only if the pair $(\mathbf{A} - \mathbf{K} \mathbf{L}, \mathbf{L})$ is uniformly observable, where \mathbf{K} can be chosen in a similar way to Section 13.4.2 in [39]. If the PE is fulfilled, from Lemma 13.4 in [39], the observability of the pair

$(\mathbf{A} - \mathbf{KL}, \mathbf{L})$ is proven and, thus, the following condition holds

$$\int_t^{t+\delta t} \dot{V}_i(\tilde{\mathbf{z}}(\sigma)) d\sigma \leq -\frac{2k_w}{\max\{\lambda_M(\mathbf{Q}), \beta\}} V_i(\tilde{\mathbf{z}}, \tilde{\boldsymbol{\chi}}). \quad (\text{A11})$$

In conclusion, (A8), (A9) and (A11) allow us to claim that both $\tilde{\mathbf{z}}$ and $\tilde{\boldsymbol{\chi}}$ are exponentially convergent to zero.

Proof of Theorem 3

In order to prove Theorem 3, it is worth defining the following Lyapunov function

$$V = V_o(\boldsymbol{\varepsilon}) + \bar{V}_i(\tilde{\mathbf{z}}, \tilde{\boldsymbol{\chi}}), \quad (\text{A12})$$

where V_o has been already defined in (61) while \bar{V}_i is a Lyapunov function satisfying the following conditions

$$c_1 \|\tilde{\mathbf{z}}\|^2 \leq \bar{V}_i(\tilde{\mathbf{z}}) \leq c_2 \|\tilde{\mathbf{z}}\|^2, \quad (\text{A13})$$

$$\dot{\bar{V}}_i \leq -c_3 \|\tilde{\mathbf{z}}\|^2, \quad (\text{A14})$$

$$\left\| \frac{\partial \bar{V}_i}{\partial \tilde{\mathbf{z}}} \right\| \leq c_4 \|\tilde{\mathbf{z}}\|, \quad (\text{A15})$$

for some positive constants c_1 , c_2 , c_3 and c_4 , and $\tilde{\mathbf{z}} = [\tilde{\mathbf{z}}^T \tilde{\boldsymbol{\chi}}^T]^T$. Since the conditions of Corollary 1 are satisfied, the exponential stability of the inner loop ensures the existence of such \bar{V}_i by virtue of Converse Theorem 3.12 in [39]. By recalling (69) and (67) together with (A13) and (A14), the exponential convergence of the whole state $[\boldsymbol{\varepsilon}^T \tilde{\mathbf{z}}^T]^T$ can be straightforwardly derived.

Proof of Theorem 4

In order to prove Theorem 4 it could be worth recalling the following lemma

Lemma 1. *Given the autonomous system*

$$\dot{\mathbf{x}} = \mathbf{f}(\mathbf{x}, \mathbf{u}), \quad (\text{A16})$$

suppose that $\bar{\mathbf{x}}$ is an asymptotically stable equilibrium of $\dot{\mathbf{x}} = \mathbf{f}(\mathbf{x}, \bar{\mathbf{u}})$, with domain of attraction \mathcal{O} , and that \mathcal{K} is a compact subset of \mathcal{O} . Let $\mathbf{x}(t)$ be a \mathcal{K} -recurrent solution of (A16) defined on $[0; \infty)$, and suppose that $\mathbf{u}(t) \rightarrow \bar{\mathbf{u}}$ as $t \rightarrow \infty$. Then, $\mathbf{x}(t) \rightarrow \bar{\mathbf{x}}$ as $t \rightarrow \infty$.

Proof. It is worth remarking that a function $x : \mathcal{D} \rightarrow \mathcal{X}$ is \mathcal{K} -recurrent if for each $T > 0$ there is some $t > T$ such that $x(t) \in \mathcal{K}$, where $\mathcal{K} \subseteq \mathcal{X}$ is a compact subset. A detailed proof can be found in [47] (see Theorem 1). \square

The two-loop dynamics (48)-(70) can be rewritten in terms of an autonomous system, analogous to (A16), with state vector $\tilde{\boldsymbol{\nu}}$ and input vector $\mathbf{J}_\zeta \ddot{\boldsymbol{\zeta}}$. If the PE condition is satisfied, from Corollary 1, $\tilde{\mathbf{z}}$ and $\tilde{\boldsymbol{\chi}}$ are exponentially convergent to zero. By virtue of Theorem 2, the nominal system, i.e., the two-loop dynamics (48)-(59) in the absence of the error $\ddot{\boldsymbol{\zeta}}$, is exponentially convergent to zero; thus, the first condition of Lemma 1 is satisfied.

By resorting to Converse Theorem 3.12 and Lemma 5.7 in [39], it is possible to state that $\tilde{\boldsymbol{\nu}}$ is norm-bounded, i.e., there exists a positive constant ρ such that $\|\tilde{\boldsymbol{\nu}}(t)\| \leq \rho, \forall t \geq 0$. In other words, $\tilde{\boldsymbol{\nu}}$ is a \mathcal{K} -recurrent solution since it never leaves the hypersphere \mathcal{K} with radius ρ , which, in turn, is a compact subset of \mathbb{R}^{2n+24} . By recalling that $\tilde{\mathbf{z}}$ and $\tilde{\boldsymbol{\chi}}$ are exponentially convergent to zero and, by virtue of (71), it can be recognized that

$\mathbf{J}_\zeta \ddot{\zeta} \rightarrow \mathbf{0}$ as $t \rightarrow \infty$. Since all conditions stated by Lemma 1 are met it can be argued that, also in the presence of the error $\ddot{\zeta}$, the equilibrium $\tilde{\mathbf{v}} = \mathbf{0}$ of the perturbed system (49), (70), is asymptotically stable.

Proof of Corollary 2

The system defined by equations (70), (55) can be viewed as the nominal system (49), (59) with two perturbation terms $\mathbf{B}(\mathbf{A}\tilde{\boldsymbol{\chi}} + \boldsymbol{\varsigma})$ and $\mathbf{J}_\zeta \ddot{\zeta}$, respectively. From (58) and (72) it can be argued that both the perturbation terms are bounded and non-vanishing, since $\boldsymbol{\varsigma}$ is bounded and $\tilde{\boldsymbol{\chi}}$ could be kept bounded by resorting to the projection operator even if PE condition cannot be met. By resorting to arguments analogous to proof of Theorem 4, it can be argued that exists a Lyapunov function that satisfies the conditions of Lemma 5.7 in [39], and, thus, it is possible to state that $\tilde{\mathbf{v}}$ is norm bounded.